NASA Technical Paper 2550

January 1986

NASA-TP-2550 19860009624

A Stochastic Model for Particle Impingements on Orbiting Spacecraft

Leonard W. Howell, Jr.

NASA

NASA Technical Paper 2550

1986

A Stochastic Model for Particle Impingements on Orbiting Spacecraft

Leonard W. Howell, Jr.

George C. Marshall Space Flight Center
Marshall Space Flight Center, Alabama

National Aeronautics and Space Administration

Scientific and Technical Information Branch

TABLE OF CONTENTS

LIST OF ILLUSTRATIONS

LIST OF ILLUSTRATIONS (Concluded)

TECHNICAL PAPER

A STOCHASTIC MODEL FOR PARTICLE IMPINGEMENTS ON ORBITING SPACECRAFT

I. INTRODUCTION

Valuable information relative to mission planning, spacecraft design, and expected performance may be gained from an investigation of the way a spacecraft interacts with its environment. Often, however, direct experimentation is not feasible and the physical setting is too complex to model deterministically. To further complicate the situation, many of the natural phenomena under investigation are best described as random processes.

For example, it may be of interest to determine the effects of meteoroids striking a spacecraft or of cosmic rays which penetrate the vehicle and affect on-board radiation sensitive equipment. Here, meteoroid flux, velocity, and direction of travel are considered to be randomly distributed with known probability distributions. Similarly, cosmic ray energies and direction of travel follow certain probability distributions.

Simulation techniques incorporating probabilistic features applicable to these scenarios are generally referred to as Monte Carlo simulations and are resorted to whenever the systems being studied are not amenable to deterministic methods or when experimentation is not feasible.

This report presents a general methodology for performing a Monte Carlo simulation of particles impinging on a spacecraft. These particles could be photons, cosmic rays, meteoroids, or particle beams and the spacecraft design is arbitrary. An example is included which illustrates this methodology.

II. STEPS IN THE MODELING PROCESS

A. Modeling Objective

An investigation, designed to assess the impact of the space environment on a spacecraft, frequently arises when spacecraft survivability or performance is threatened. This is particularly true today because many spacecraft scheduled for in-orbit operation during the next decade will have several hundred square meters of exposed surface area which greatly increases the expected number of particle strikes. Based on the spacecraft design, mission, and sensitivity to particle impingements, various modeling goals might arise. In the case of meteoroids, for example, the modeling objective might be: (1) How many meteoroids larger than a certain size will hit the spacecraft during its planned lifetime? (2) What is the probability of a certain spacecraft module being punctured? (3) How are sensitive components "shadowed" by the rest of the vehicle and thus better protected? (4) What does a typical time profile of angular momentum transfers caused by the impacts look like and will they cause pointing disturbances of on-board telescopes?

These are just a few of the questions that might arise and fit nicely into a simulation environment. Obviously, simulations of this type require a geometrical model of the spacecraft. The level of detail that one builds into the geometrical model is dependent on the modeling objective in terms of accuracy desired and available resources, e.g., manpower, computer facilities, and time constraints.

Thus, one should first have a well-defined modeling objective which will then determine the degree of detail required in the geometrical model. Also, the computer program should be flexible enough so that greater detail in the geometrical model can be added at a later time should the objective be further refined.

B. Geometrical Model of the Spacecraft

The shape of the spacecraft largely determines the complexity of the simulation model. A vehicle which has a convex shape, such as a sphere or cube, is the easiest type to model. Because each surface element is exposed to 2π steradian of space, there will not be a shadowing effect. Furthermore, if the particle flux is isotropic, random points uniformly distributed over the surface may be chosen by Monte Carlo methods to represent the impact points. Random direction cosines may then be simulated as well as the physical properties of the impinging particles, e.g., mass, charge, and velocity. With this information the effects of the simulated impact can be determined using physical laws.

In general, however, the vehicle shape is much more complex and not convex, so that many surface elements are shaded by other parts of the vehicle. Thus, these shadowed surfaces are hit less frequently on the average. Therefore, in order to include the realistic effects of shadowing in the simulation, more elaborate techniques must be employed to obtain the correct distribution of impact coordinates and associated direction cosines over the surface of the spacecraft.

To solve this problem, it is first necessary to determine the point at which the particle's trajectory intersects convex generic objects, such as cylinders and boxes, having arbitrary position and orientation relative to some coordinate frame. Using these generic shapes, a geometrical model can be assembled which adequately resembles the spacecraft with the level of detail being dependent upon the modeling objective. Thus, an impingement on the vehicle is determined by impingements on each of the components used to construct the model. If more than one component intersects a particle trajectory, the impact coordinates of the component which was struck first can be chosen as the point of intersection of the trajectory and the spacecraft. Consequently, this approach automatically solves the shadowing problem and provides the correct distribution of impact coordinates and associated direction cosines over the surface of the spacecraft.

In the event that the particle reflects or penetrates, its subsequent trajectory and any secondary impacts can be determined in a similar manner.

The following generic objects were chosen as the basic building blocks for spacecraft geometrical models: (1) sphere, (2) cone, (3) cylinder, (4) box, (5) cap from a sphere, (6) frustum, (7) paraboloid, and (8) ellipsoid.

These objects can be used to describe most vehicles that one is likely to encounter; unusual shapes can be created by merging combinations of these figures together when necessary.

The intersection of a line in space with these generic objects can then be programmed. Figures 1 and 2 are stereoscopic pairs (Appendix A) which illustrate lines in space originating from a central source, some of which "strike" the objects suspended vertically. Strikes are easily spotted by the solid line intersecting the surface of the object and then continued by a dotted path after the point of impact. Those lines which do not hit any of the objects are thereby easily distinguished from those that do.

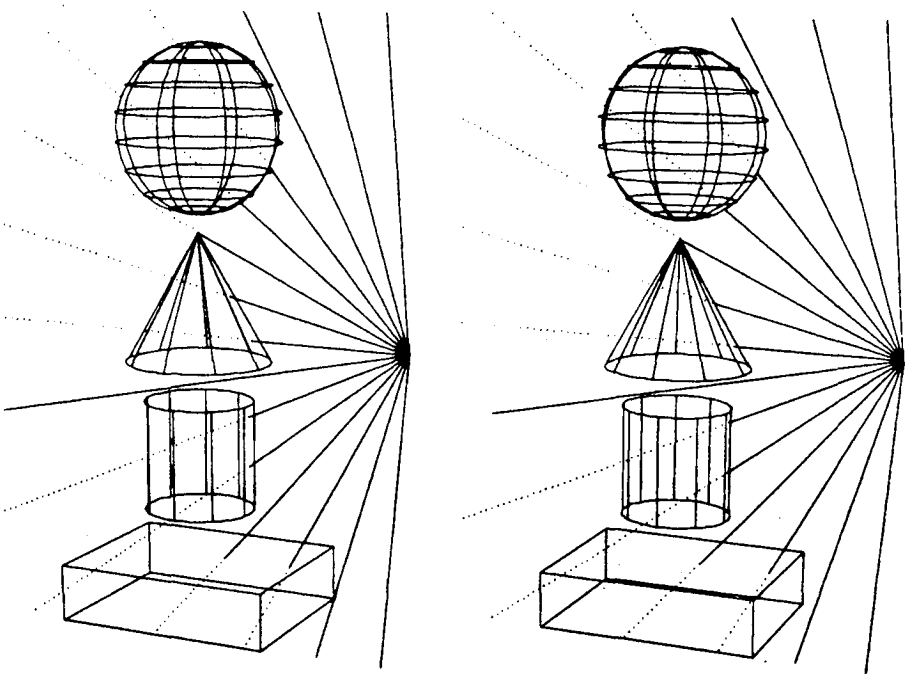

Figure 1. Intersection of lines in space with a sphere, cone, cylinder, and box.

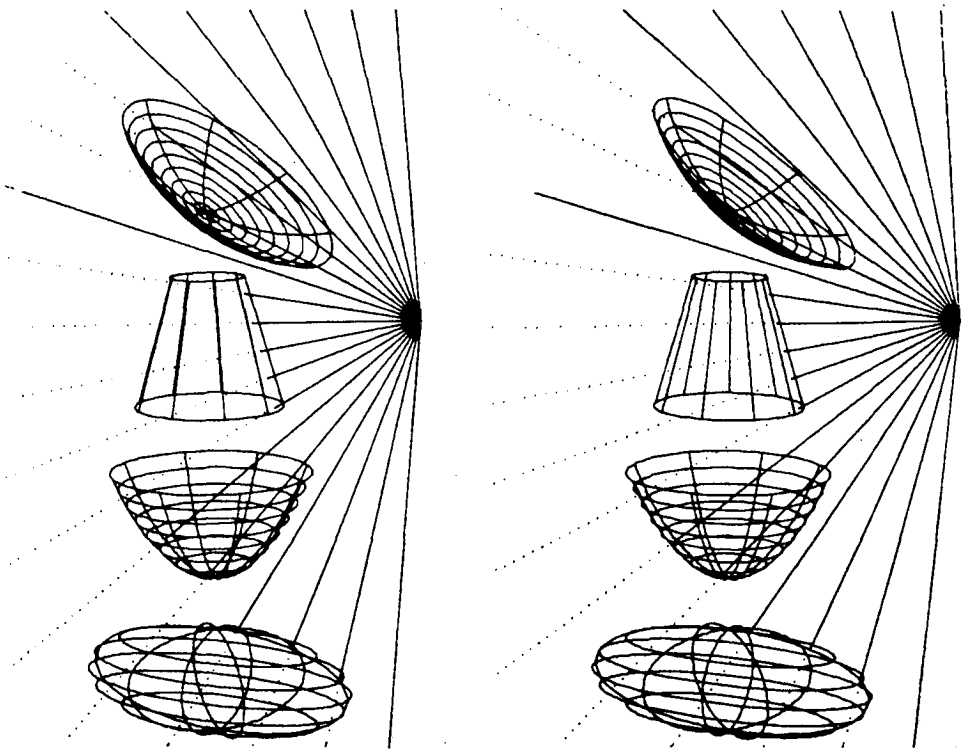

Figure 2. Intersection of lines in space with a spherical cap, frustum, paraboloid, and ellipsoid.

For purposes of verifying the mathematics and computer programming, it is convenient to initially have control over the direction of the particle trajectories. Thus, one can "take aim" at an object and check to see that the programmed model performs correctly. A system of spraying in a specified plane may also be incorporated which permits multiple checks as illustrated in many of the figures in this report.

Figures 3, 4, and 5 depict assembled geometrical models. Figure 3 shows a model of the Hubble Space Telescope. Its exposure to meteoroid impingements and their resulting angular momentum transfers are investigated in the example in Section III. Figure 4 represents the detector of a cosmic ray instrument to be part of the Burst and Transient Source Experiment on the Gamma Ray Observatory.

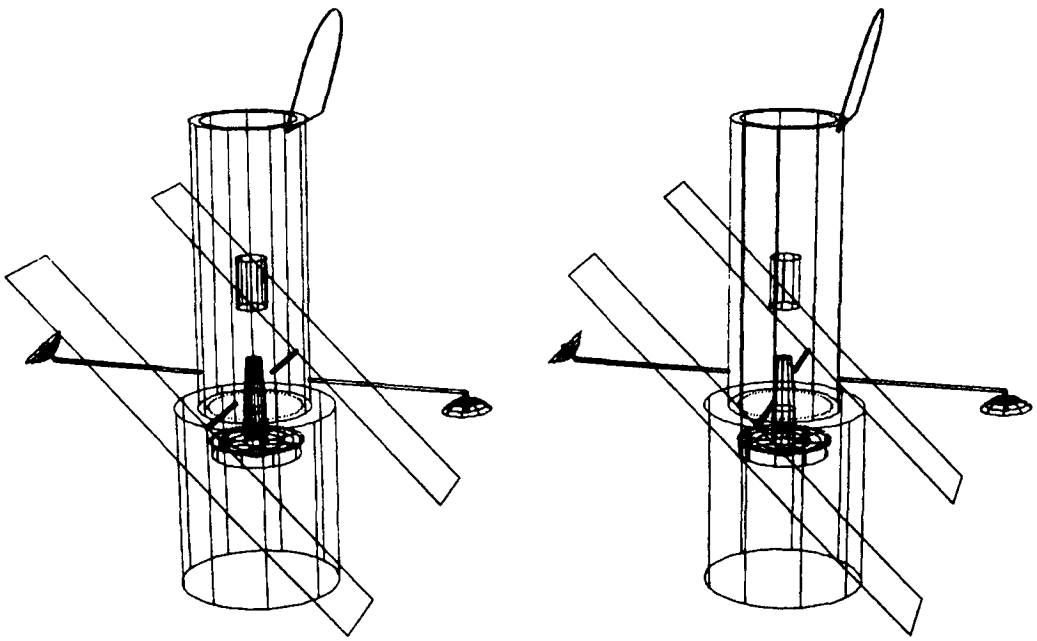

Figure 3. Geometrical model of the Hubble Space Telescope.

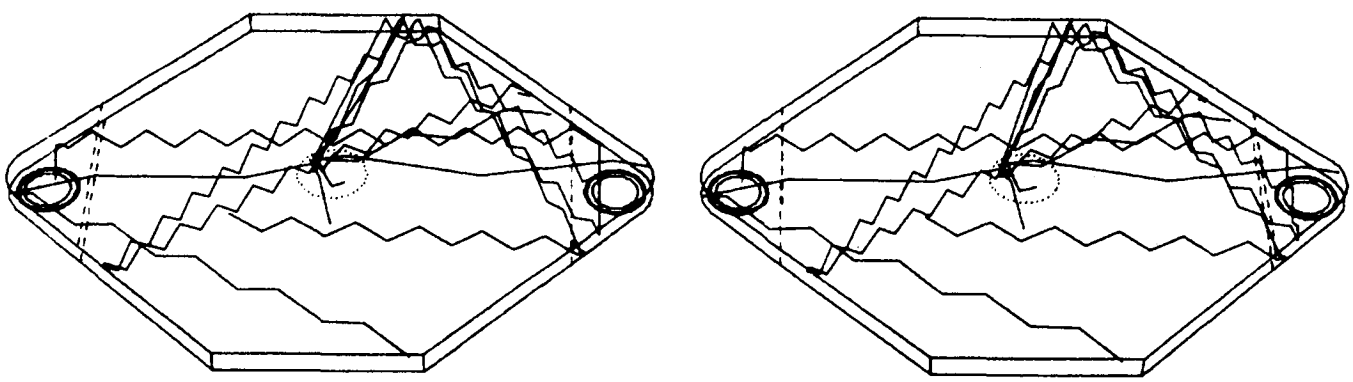

Figure 4. Fluorescence caused by a proton passing through the cosmic ray detector assembly.

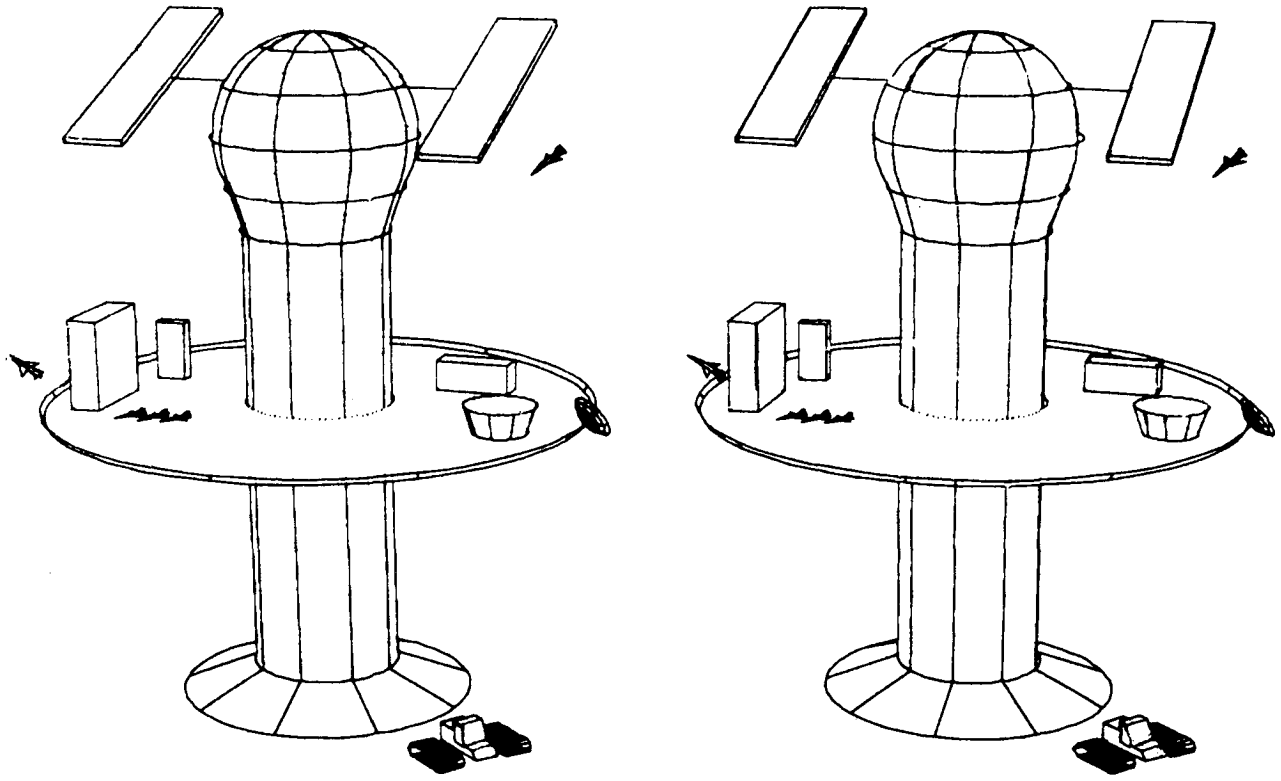

Figure 5. Space City.

A simulated proton passing vertically through the assembly causes fluorescence photons to be emitted, the paths and reflections of which are illustrated by the lines within the detector. This model assisted in a study of the distribution of fluorescence photons collected by each photomultiplier tube located in the "ears" of the assembly and helped determine their optimal locations, the effect of a reflecting foil around the perimeter of the detector, and other parameters of interest. Figure 5 is a futuristic "space city" and has been included to illustrate the flexibility of these methods. Particle impingements not shown in this example could represent meteor storms or cosmic rays.

C. Simulation of the Particle and the Space Environment

Once the geometrical model has been constructed and the program written to determine the points at which particle trajectories intersect the model, we are ready to simulate the space environment. Here, one must model the behavior of the particles of interest: What is the distribution of the particle mass and/or change? What is their flux distribution and what energies do they possess? Is it an isotropic flux or is there an emitting source(s)?

Distributions for these properties are usually available in the literature or from researchers in the relevant field. These can be normalized if necessary and then used in the simulation to generate the appropriate characteristics of each simulated particle.

To simulate the spacecraft in its space environment, it suffices to choose a volume of space, such as a sphere or cube, that can contain the geometrical model of the spacecraft, and then consider the particle flux in this region. Since we wish to obtain as many simulated hits as possible, the dimensions

of the region of space should be chosen so that the spacecraft geometrical model barely fits in order to maximize the number of simulated trajectories which intersect the vehicle, thereby optimizing computer time.

Many particle fluxes of interest are considered to be isotropic, a property which unfortunately is the most difficult to simulate. A physical example of what is meant by isotropic flux is that the faces of a cube would each be hit statistically the same number of times, independent of the position and orientation of the cube in space.

In order to simulate the isotropic flux of particles, one must simulate random lines through the region of space which contains the spacecraft geometrical model. A natural choice for the volume of space is a sphere and thus, one must generate random chords in the sphere to simulate the flux.

Many methods can be devised which generate random chords in a sphere. For instance, two random points uniformly distributed over the surface of the sphere can be connected and thus define a random chord. However, this procedure is such that when a cube moves from the center of the sphere to the surface, it will be hit more often. A more elaborate method first picks a random point uniformly distributed on the surface of the sphere. This point can be associated with the simulated particle's entry point into the sphere. Since the particle's direction of travel is isotropic, we can imagine a unit sphere with center at the previously selected random point; picking another random point on the surface of the unit sphere would give a direction of travel for the particle (either into or out of the sphere) and would thus define a random chord. However, this method also produces a radial density in the sphere, although not as pronounced as the first method discussed.

In order to simulate the desired properties of isotropic flux, we proceed as follows. Consider a sphere of radius R centered at the origin. We will develop the methods for simulating isotropic flux in the sphere by first considering the particle's entry point on the sphere fixed and simulate its direction of travel and thus its exit point from the sphere. This chord thus defined will then be randomly oriented in such a way that the particle entry point (and exit point) is uniformly randomly distributed over the surface of the sphere.

Let P = (0, -R, 0) be the entry point and consider another sphere of radius r less than R inside the first sphere and centered at the origin. Now, in the y-z plane [Fig. 6(a)], the chord PQ intersects the smaller sphere if and only if the point Q is in the cap of the sphere defined by the inner sphere's "shadow" as viewed from P. Thus, the probability of a hit is equal to the probability that the exit point is contained in the shadowed area S. Writing this in terms of the elevation angle (90 deg - the angle of incidence), we have:

$$P(\theta_1 \leqslant \theta_1) = Pr(Q \in S) = (2\pi\ R(R-R\cos 2\theta_1)/4\pi\ R^2) = \sin^2 \theta_1$$

Thus, by the inverse cumulative distribution method, a random elevation angle $\theta_1 = \sin^{-1} U_1^{1/2}$, where U_1 (and all subsequent U's) will denote pseudo-random numbers uniformly distributed between zero and one, is generated. This defines an exit point in the y-z plane as $(0, R\cos 2\theta_1, R\sin 2\theta_1)$. Since the y-z plane is an arbitrary slice of the sphere, one must provide a random uniform 2π rotation about the y-axis [Fig. 6(b)] which gives:

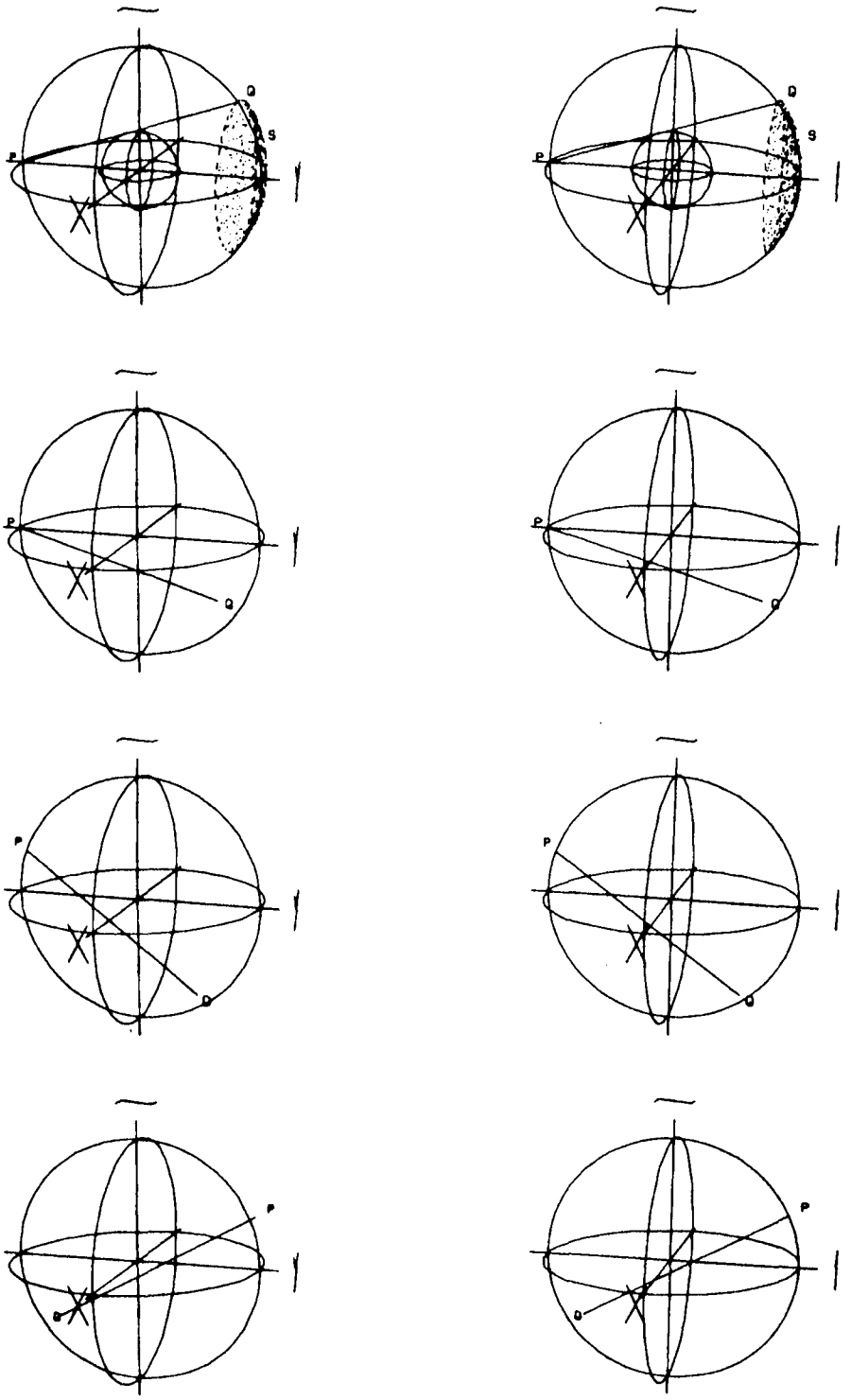

FIGURE 6A. RANDOM ELEVATION ANGLE
FIGURE 6B. RANDOM ROTATION ABOUT THE Y–AXIS
FIGURE 6C. RANDOM ROTATION ABOUT THE X–AXIS
FIGURE 6D. RANDOM ROTATION ABOUT THE Z–AXIS

Figure 6. Simulation of isotropic flux.

$$Q = \begin{bmatrix} \cos\theta_2 & 0 & -\sin\theta_2 \\ 0 & 1 & 0 \\ \sin\theta_2 & 0 & \cos\theta_2 \end{bmatrix} \begin{bmatrix} 0 \\ R\cos 2\theta_1 \\ R\sin 2\theta_1 \end{bmatrix} ,$$

where $\theta_2 = 2\pi\, U_2$.

This determines the direction of travel for a given particle having the desired isotropic flux properties. Since the entry point must now be uniformly randomly distributed over the surface of the sphere, the following rotations are applied to the chord PQ. A rotation θ_3 about the x-axis [Fig. 6(c)] defined by $\theta_3 = \sin^{-1} 2(U_3-0.5)$, followed by a random uniform 2π rotation about the z-axis [Fig. 6(d)] (Appendix C of Reference 2 gives the mathematical proof). Thus the entry point is given by

$$P = \begin{bmatrix} \cos\theta_4 & \sin\theta_4 & 0 \\ -\sin\theta_4 & \cos\theta_4 & 0 \\ 0 & 0 & 1 \end{bmatrix} \begin{bmatrix} 1 & 0 & 0 \\ 0 & \cos\theta_3 & \sin\theta_3 \\ 0 & -\sin\theta_3 & \cos\theta_3 \end{bmatrix} \begin{bmatrix} 0 \\ -R \\ 0 \end{bmatrix}$$

and the exit point by

$$Q = \begin{bmatrix} \cos\theta_4 & \sin\theta_4 & 0 \\ -\sin\theta_4 & \cos\theta_4 & 0 \\ 0 & 0 & 1 \end{bmatrix} \begin{bmatrix} 1 & 0 & 0 \\ 0 & \cos\theta_3 & \sin\theta_3 \\ 0 & -\sin\theta_3 & \cos\theta_3 \end{bmatrix} \begin{bmatrix} \cos\theta_2 & 0 & -\sin\theta_2 \\ 0 & 1 & 0 \\ \sin\theta_2 & 0 & \cos\theta_2 \end{bmatrix} \begin{bmatrix} 0 \\ R\cos 2\theta_1 \\ R\sin 2\theta_1 \end{bmatrix}$$

Generating random chords by this method in the Monte Carlo simulation will produce the desired isotropic flux in the sphere containing the spacecraft geometrical model. Points of impact and direction cosines for trajectories which intersect the spacecraft model may then be used, along with information about the particle and the struck component of the spacecraft to simulate the effect of the impact.

Flux models found in the literature will normally be given in the units "number of particles of mass m or greater per square meter per second." If the spacecraft is convex, one simply multiplies the flux distribution by the surface area of the spacecraft to obtain the expected frequency of hits. For non-convex shapes, the effective surface area may be estimated by placing the geometrical model of the spacecraft inside a convex region having surface area S and then simulating N random trajectories through the region. If n of these trajectories intersect the geometrical model, then the approximate effective surface area of the spacecraft is given by nS/N. Furthermore, a $100(1-\alpha)$ percent confidence interval for the effective surface area A, using the Gaussian approximation to the Binomial distribution, is defined by the probability

$$\Pr[S(p - Z_{\alpha/2}((p(1 - p)/N)^{1/2}] \leqslant A \leqslant S(p + Z_{\alpha/2}(p(1 - p)/N)^{1/2})] = 1 - \alpha \quad ,$$

where $p = n/N$ and $Z_{\alpha/2}$ is the percentile point for the Gaussian distribution.

The flux for particles may require further modification due to the spacecraft's proximity to the Earth. For example, Reference 1 gives an Earth shielding factor which modifies the flux of sporadic meteoroids at an altitude H above the surface of the Earth and uses the formula

$$S = (1 + \cos \theta)/2 \quad ,$$

where $\theta = \sin^{-1} [R/(R + H)]$ and R is the radius of the Earth.

A gravitational defocussing factor is also used to modify the flux of the meteoroids and is given by

$$G = 0.57 + 0.43 \ (R + H)/R \quad .$$

This is necessary because the flux model for sporadic meteoroids was developed for a specific altitude which is gravitationally enhanced relative to higher orbits.

After the flux has been adjusted for the proper orbit of the spacecraft and any other necessary modifications made, it can be multiplied by the effective spacecraft surface area A to give the expected frequency f of particle impingements.

If one wishes to simulate the spacecraft in its space environment for a specified time T, assume that the distribution of the time between hits follows an exponential distribution with parameter f and that the distribution of hits during the time interval of length T follows the Poisson distribution with parameter fT. Therefore, there will be N particle impingements, where N is determined by

$$\sum_{i=1}^{N} t_i \leqslant T \quad \text{and} \quad \sum_{i=1}^{N+1} t_i > T \quad ,$$

and t_i is simulated as $t_i = -(\ln U_i)/f$.

Proceeding in this manner, a representative sample of particle impingements for the time interval of length T may be obtained.

D. Particle Impact and Subsequent Events of Interest

This section deals with the events which motivated the modeling effort, and it is the cumulative statistics that are gathered here that will hopefully satisfy the modeling objective.

Up to this point, a simulated particle with its characteristics of interest, its impact point on the spacecraft, and direction cosines for the trajectory of the particle relative to a coordinate frame in the region of space containing the geometrical model has been generated.

The physics of what happens at the point of impact and any secondary events which then occur must now be modeled. This requires the availability of the appropriate physical models which mathematically describe the impact and any subsequent events of interest. Inputs to these physical models will be the impact coordinates, direction cosines of the trajectory, angle of incidence, mass, velocity, etc., of the simulated particle and the thickness, composition, and geometry of the spacecraft component that was hit. The output will be the effect of the simulated impact, such as momentum transfer, penetration depth, and energy deposition as predicted by the physical models.

Unfortunately, however, the choice of which physical models to use is not always clear-cut and compromises must often be made. Such situations might arise when the available physical model was empirically fit using experimental results in which the particles, targets, velocities, mass, etc., differ somewhat from those to be encountered in the present application or when the model is so complex that a simpler, yet adequate, model is preferred.

Some modeling objectives will be focussed on the secondary events which follow the particle impact and may become quite involved. For example, in the cosmic ray detector simulation, the majority of the modeling effort was concerned with the physical events which occurred after cosmic ray impact. Here the charged particle was assumed to traverse a linear path through the detector. Based on its pathlength, simulated energy deposition and incident particle charge, fluorescence photons are emitted from random points along the cosmic ray trajectory through the detector. These fluorescence photons are assumed to be emitted isotropically with no preferred direction of travel. Based on the laws for internal reflection of light having perpendicular and parallel polarization, the photons are either reflected or transmitted each time the photon reaches a glass-"air" interface. Also, photons can be absorbed or strike one of the photocathodes in the ears of the assembly, the latter registering as a photon count in the struck photomultiplier tube. Many other relevant physical properties were included in the simulation which made the subsequent events following cosmic ray impact the primary focus of the modeling effort.

In these situations, one must be careful to keep a balance between detail and computer run time; otherwise a very sophisticated model may result which, unfortunately, may not produce enough output to be useful.

E. Results of the Simulation

As previously discussed, a representative sample of particle impingements and their simulated effects may be obtained for a time interval of length T which will usually be the planned lifetime of the spacecraft. Obviously, repeated simulations of these impingements over the time interval T will produce different results. Combining results from many such runs, or what really amounts to the same as eliminating the variable time from the simulation, will provide a large amount of simulated data.

Frequency statistics will be maintained for the simulated data of interest from which a frequency histogram can be constructed. If necessary, the Monte Carlo study can be continued until the histogram assumes a non-varying shape which will likely occur when the data is two-dimensional. This histogram will be used to approximate the probability distribution associated with the variables under investigation, from which the desired inferences may be based.

The example presented in the next section will illustrate these methods.

III. EXAMPLE: METEOROID IMPINGEMENTS ON THE HUBBLE SPACE TELESCOPE

A. Modeling Objective

The pioneering observatory, Hubble Space Telescope (HST), is scheduled for operation in Earth-orbit beginning in mid-1986.

For the HST to perform its mission, very accurate line-of-sight stability must be maintained for periods up to 10 hr. To maintain this stability, the attitude information is provided by two on-board Fine Guidance Sensors (FGSs) (a third FGS is either on stand-by or it is performing astrometry). The FGSs track guide-stars through the main telescope; pointing stability is maintained while the FGSs stay locked onto the guide-stars.

Because of the telescope exposure to meteoroids in its space environment, concern arose over the possibility that angular momentum transfers caused by meteoroid impingements would cause a FGS loss-of-lock which would result in a telescope pointing disturbance.

Thus, the modeling objective is to investigate the expected angular momentum transfers caused by meteoroids impinging on the HST and to assess their detrimental effects on the pointing accuracy of the telescope.

B. Geometrical Model of the Telescope

Based on the degree of detail desired for the HST model, it was decided that most components of the telescope could be represented by right circular cylinders, cylindrical shells, frustums, boxes, and paraboloids. Table 1 gives the modeled components and appropriate parameters.

Using these building blocks, construction of the telescope model began. Figure 7 shows the telescope aft shroud modeled as a cylinder and the primary mirror as a cylinder whose top has been replaced by a paraboloid. The central baffle is modeled as a frustum sitting on top of a cylinder. Note the hole in the mirror and various points at which the lines (trajectories) intersect these components.

Continuing in this fashion, the Hubble Space Telescope geometrical model was assembled. Figure 8 depicts the entire model (interior components also shown) being sprayed from above. Note those trajectories which traverse the light shield and strike the secondary baffle which thereby shadowed the primary mirror.

Figure 9 shows the telescope from a different vantage point with the interior suppressed. Note that the solar arrays have been rotated and the aperture door partially closed. The top most antenna has also been pointed elsewhere.

C. Simulation of Meteoroids

1. General

Meteoroids are solid particles moving in interplanetary space and originate from both cometary and asteroidal sources.

TABLE 1. MODELED COMPONENTS AND APPROPRIATE PARAMETERS

Telescope Component	Quantity	Generic Shape	Parameter (m)
Aft shroud	1	Cylinder	R = 2.172, H = 5.061
Light shield	1	Cylindrical shell	R_1 = 1.263, R_2 = 1.524, H = 7.855
Aperture door	1	Cylinder and box	(R = 1.524, H = 0.381) half of which coincides with a box of dimension 2R, R, H
Solar panel	2	Box	2.348 by 12.111 by 0.007
Solar array boom	2	Cylinder	R = 0.051, H = 2.123
Antenna boom	2	Box	0.043 by 4.361 by 0.158
Antenna hinge	2	Cylinder	R = 0.051, H = 0.158
Antenna dish	2	Paraboloid	$z = m(x^2 + y^2)$, m = 0.76 $x^2 + y^2 \leqslant 0.42$
Antenna feedhorn	2	Cylinder	R = 0.051, H = 0.381
Secondary mirror baffle	1	Cylinder	R = 0.396, H = 1.345
Central baffle	1	Cylinder and frustum	(R = 0.298, H = 0.971) and R = 0.298, R = 0.196, H = 1.437
Primary mirror	1	Paraboloid	$z = m(x^2 + y^2)$, m = 0.048 $x^2 + y^2 \leqslant 1.44$

Based on the minimum angular momentum transfer of concern, this report treats only the meteoroid environment of cometary origin in the mass range 1E-6 to 1 gram at one astronomical unit (1 AU) from the Sun near the ecliptic plane. In this region the contribution of asteroidal particles to the total meteoroid population is considered to be negligible.

Meteoroids are classified as sporadics when their orbits are random and as streams (or showers) when a number of meteoroids have nearly identical orbits.

2. Meteoroid Speed Distribution

The geocentric speed of meteoroids ranges from 11 to 72 km/s. The lower limit corresponds to the gravitational potential of the Earth; the upper limit is the summation of the Earth speed and the maximum speed of a particle in retrograde solar orbit. The associated probability density function for sporadic meteoroid speeds is given in Figure 10. The second peak around 60 km/s corresponds to those particles in retrograde orbit.

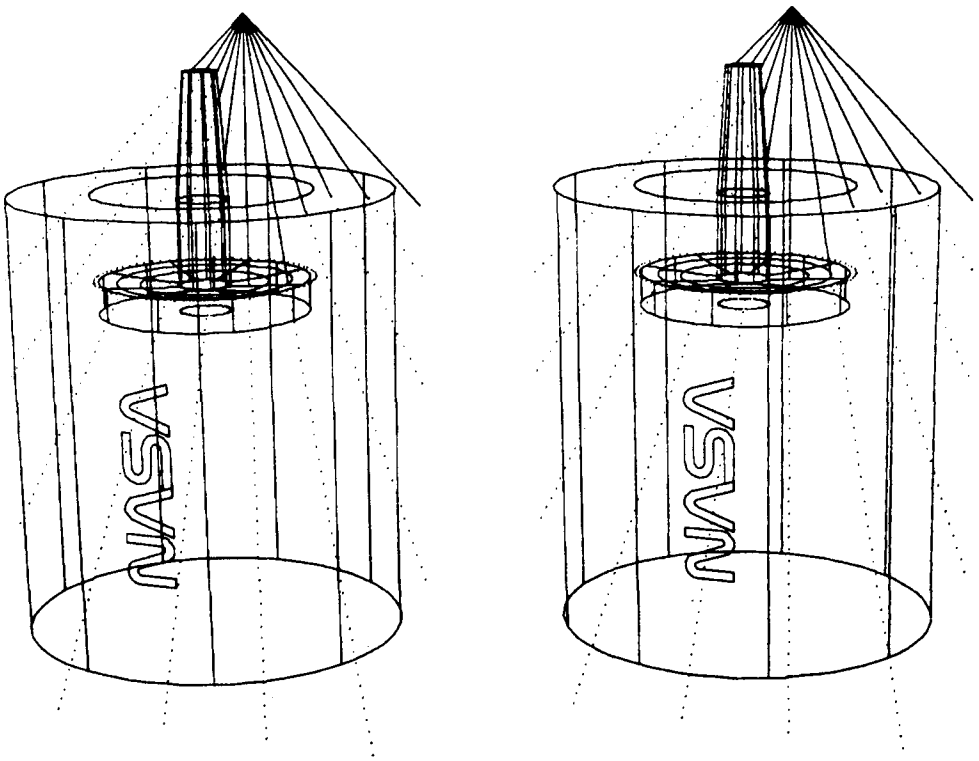

Figure 7. Trajectories intersecting the aft shroud and primary mirror of the Hubble Space Telescope.

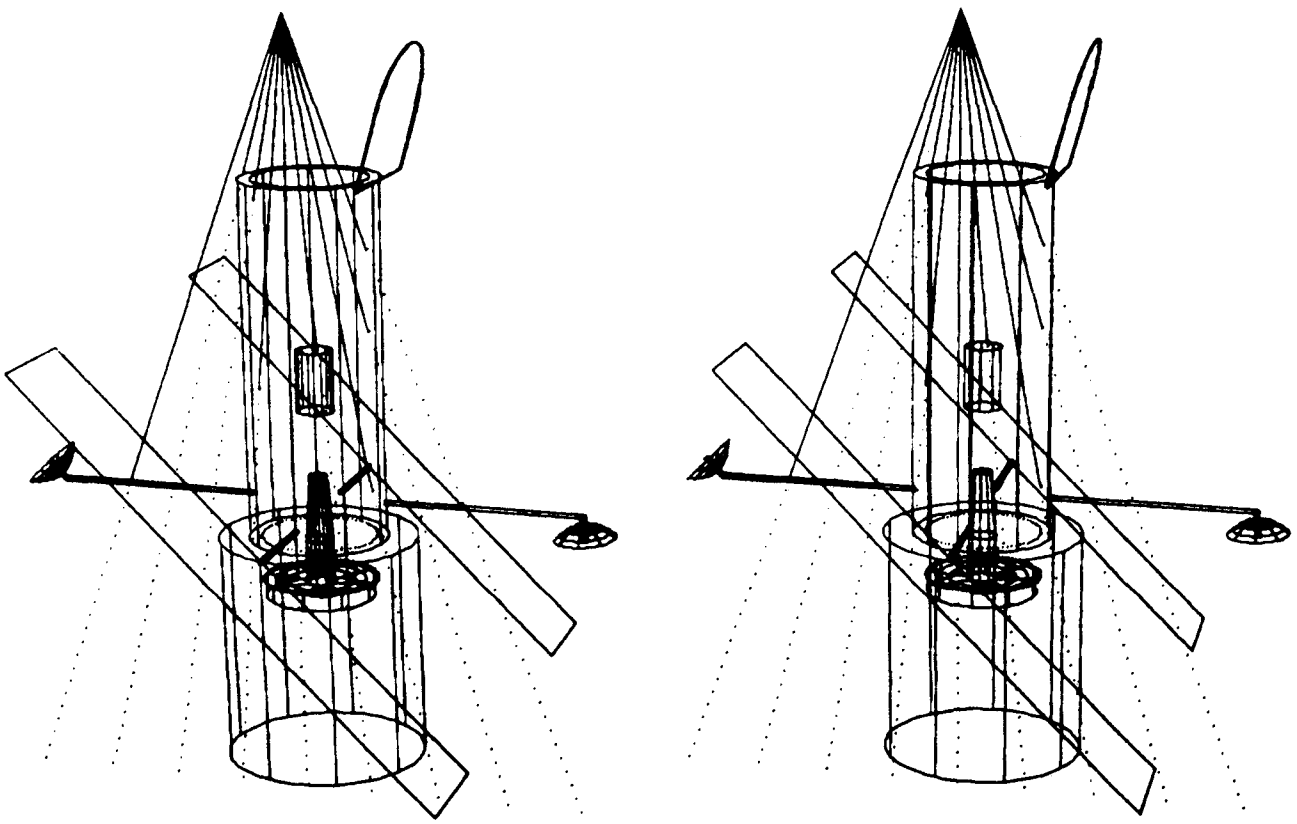

Figure 8. Hubble Space Telescope geometrical model.

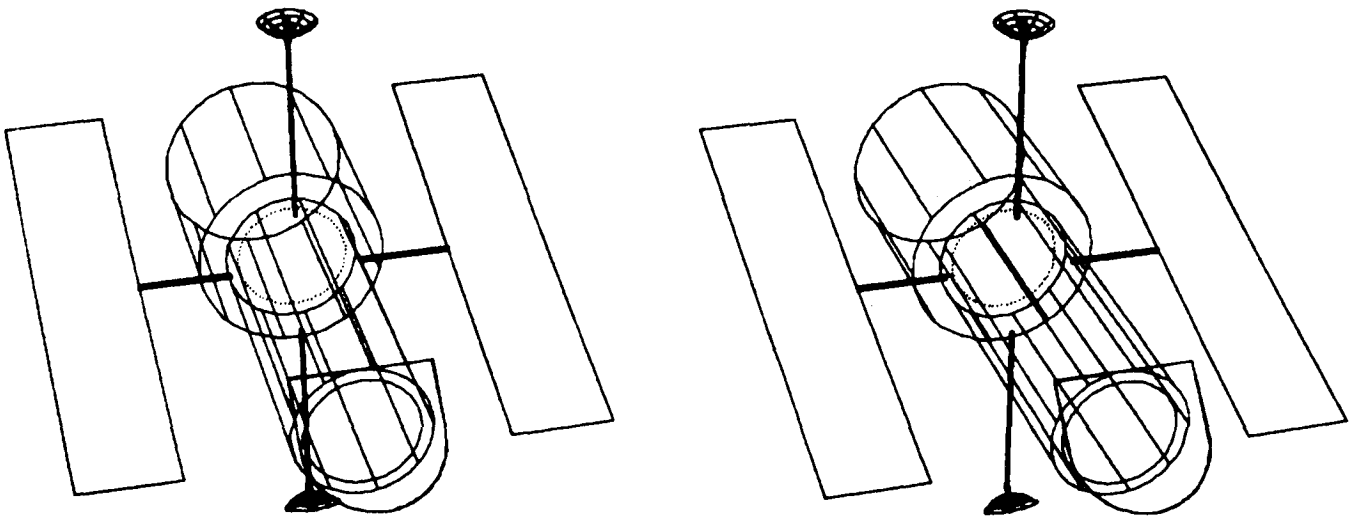

Figure 9. View of the HST geometrical model from a different vantage point; solar arrays, aperture door, and top-most antenna have been rotated.

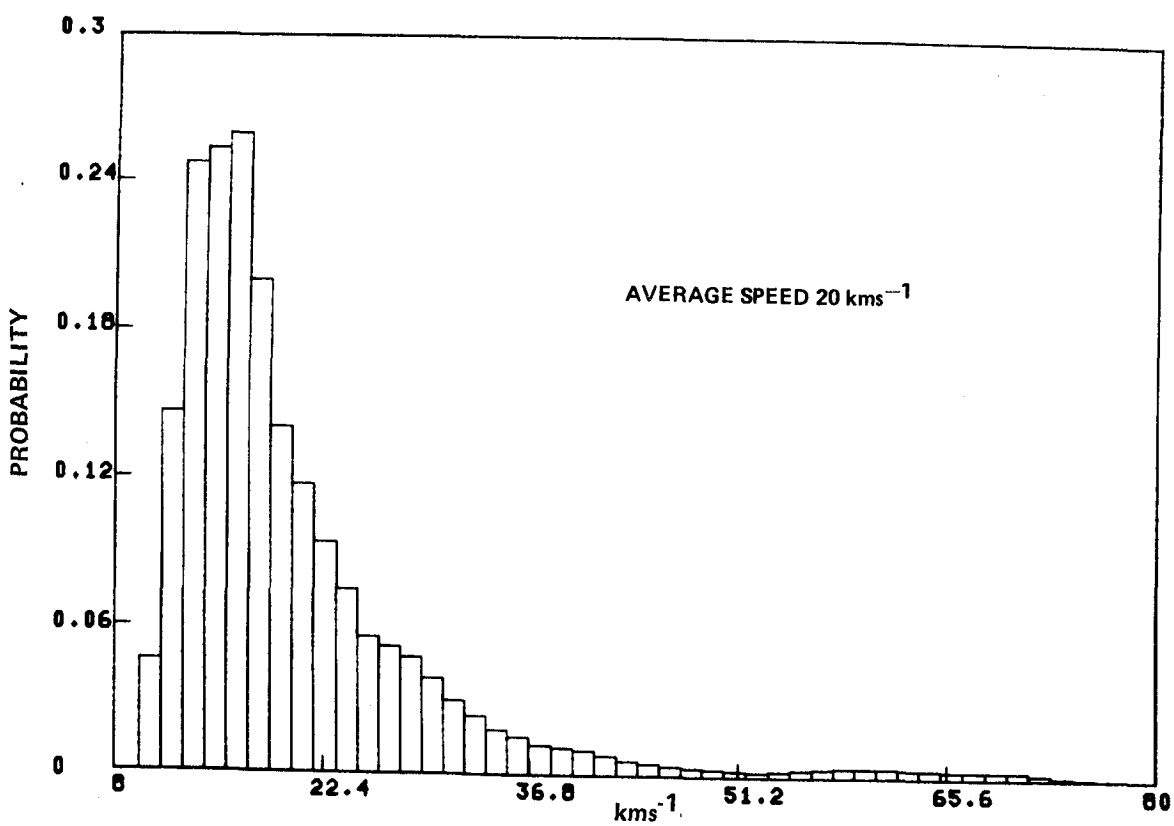

Figure 10. Sporadic meteoroid speed probability density function.

The orbital velocity of the telescope is assumed to have an average effect of zero since the telescope is equally likely to be pointing in any direction and the meteoroids strike isotropically.

3. Meteoroid Density

The cometary meteoroid has been described as a conglomerate of dust particles bound together by frozen gasses and a density value of 0.5 gm/cm^3 is used [1].

4. Meteoroid Flux

Cour-Palais [1] gives the average cumulative sporadic flux-mass model for 1 AU as

$$\log_{10} N_{SP} = -14.41 - 1.22 \log_{10} m \quad , \quad 1E\text{-}6 \leqslant m \leqslant 1 \text{ gram}$$

where N_{SP} is the number of particles of mass m (grams) or greater per square meter per second. This is then converted into the sporadic meteoroid mass distribution as depicted in Figure 11(a). The vertical line at $\log_{10} m = -6$ corresponds to the mass at which smaller masses can produce no disturbance in the pointing of the telescope. The corresponding probability distribution for sporadic meteroids in the range 1E-6 to 1 gram is depicted in Figure 11(b).

Increases in hourly rate of meteor activity can be observed at regular intervals during the calendar year. These increases in meteor activity are caused by the Earth's orbit intersecting various stream orbits throughout the year. Table 2 gives the velocity and periods of occurrence of 18 of the more prominant streams.

Also included is an activity ratio F, defined as the ratio of the cumulative flux of each stream to the average cumulative sporadic flux for mass greater than 0.1 grams. The activity ratios for each of the streams are depicted in Figure 12.

The corresponding flux mass model for stream meteoroids is [1]:

$$\log_{10} N_{ST} = -14.41 - \log_{10} m - 4 \log_{10} (V_{ST}/20) + \log_{10} F$$

where

N_{ST} = number of stream particles of mass m or greater per square meter per second

m = particle mass in grams, $1E\text{-}6 \leqslant m \leqslant 1$

V_{ST} = geocentric velocity of each stream in km/sec from Table 2

F = integrated average ratio of cumulative flux of stream to the average cumulative sporadic flux as calculated from Figure 12.

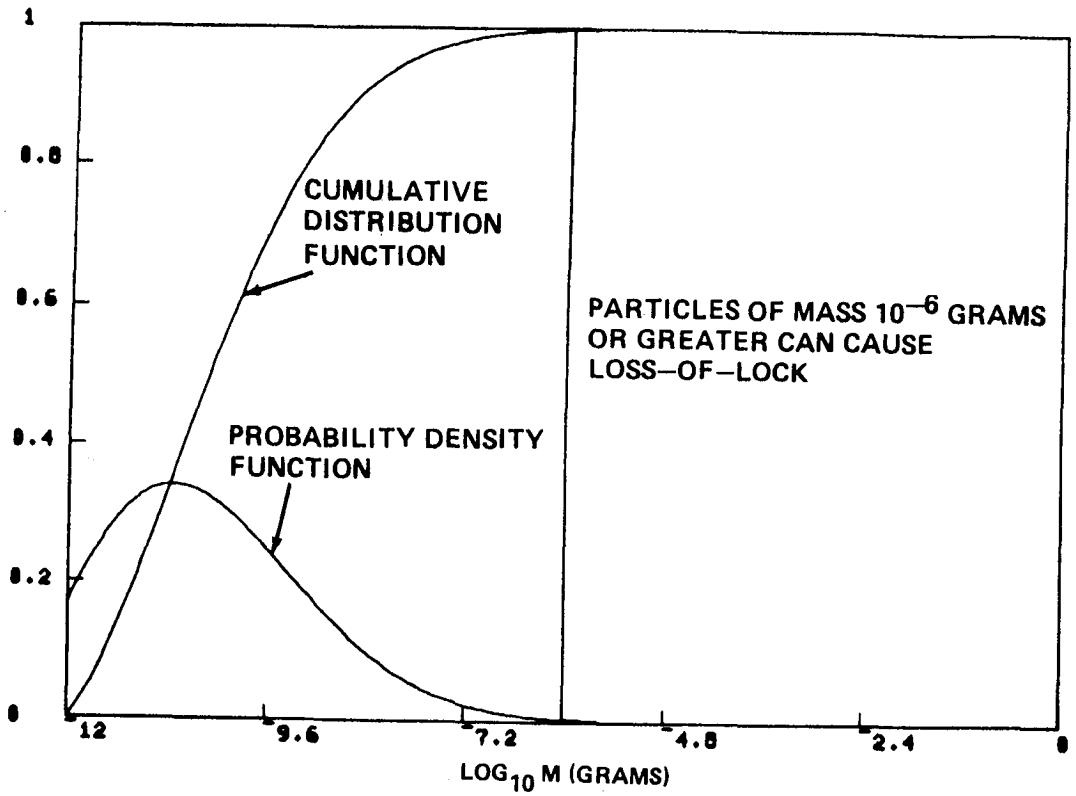

Figure 11(a). Sporadic meteoroid mass ($\log_{10}$) probability distribution.

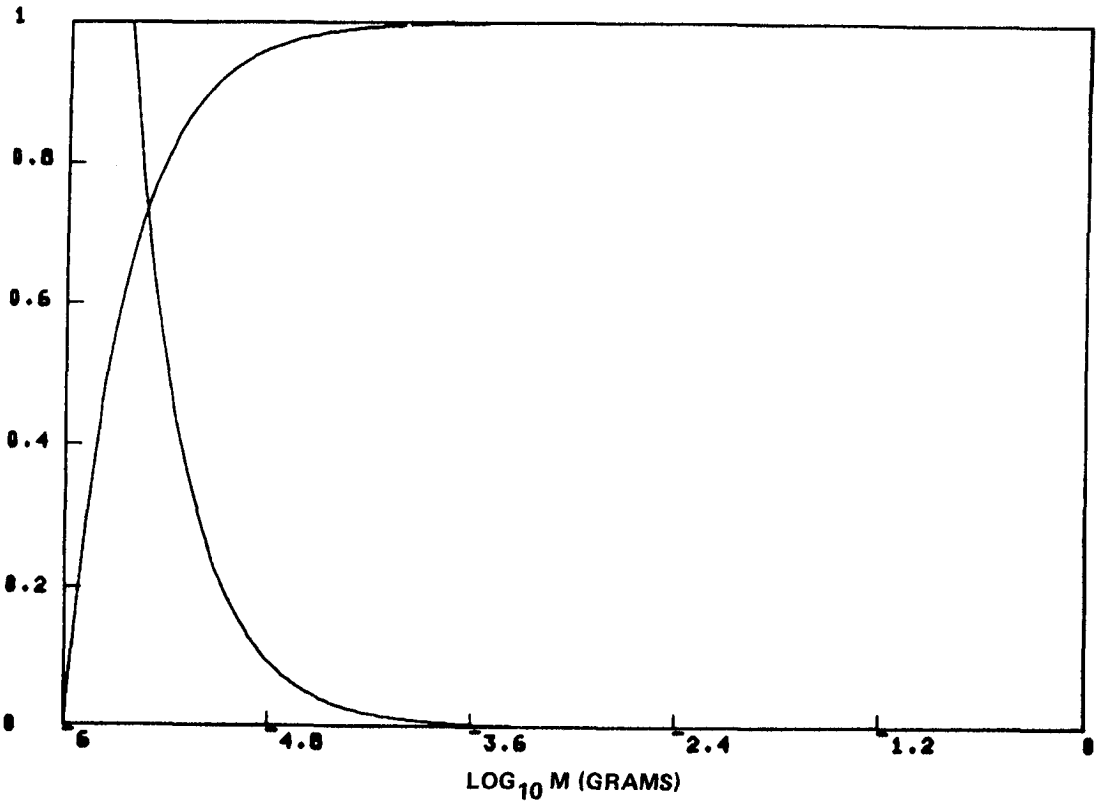

Figure 11(b). Sporadic meteoroid mass ($\log_{10}$) probability distribution for particles which can cause loss-of-lock.

TABLE 2. MAJOR METEOR STREAMS

Name	Period of Activity	Date of Maximum	F_{max} (a)	Velocity Geocentric, km/sec
Quadrantids	January 2 to 4	January 3	8.0	42
Lyrids	April 19 to 22	April 21	0.85	48
η-Aquarids	May 1 to 8	May 4 to 6	2.2	64
o-Cetids	May 14 to 23	May 14 to 23	2.0	37
Arietids	May 29 to June 19	June 6	4.5	38
ζ-Perseids	June 1 to 16	June 6	3.0	29
β-Taurids	June 24 to July 5	June 28	2.0	31
δ-Aquarids	July 26 to August 5	July 28	1.5	40
Perseids	July 15 to August 18	August 10 to 14	5.0	60
Orionids	October 15 to 25	October 20 to 23	1.2	66
Arietids, southern	October 1 to November 28	November 5	1.1	28
Taurids, northern	October 26 to November 22	November 10	0.4	29
Taurids, night	November 1 to November 30	November 15	1.0	37
Taurids, southern	October 26 to November 22	November 5	0.9	28
Leonids, southern	November 15 to 20	November 16 to 17	0.9	72
Bielids	November 12 to 16	November 14	0.4	16
Geminids	November 25 to December 17	December 12 to 13	4.0	35
Ursids	December 20 to 24	December 22	2.5	37

(a) F_{max} = ratio of maximum cumulative flux of stream to average cumulative sporadic flux.

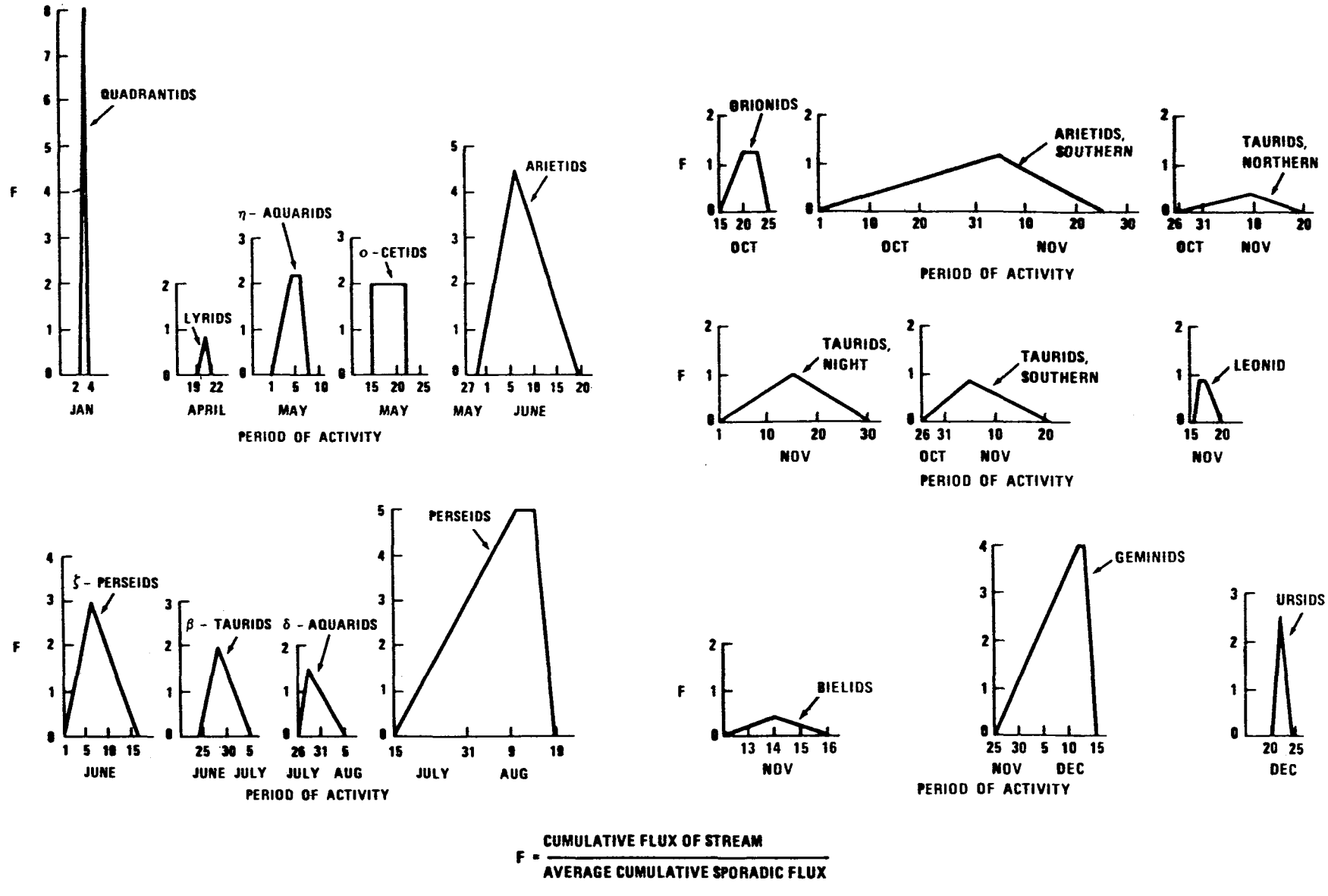

$$F = \frac{\text{CUMULATIVE FLUX OF STREAM}}{\text{AVERAGE CUMULATIVE SPORADIC FLUX}}$$

Figure 12. Activity ratio factor versus period of activity (September-December) for major streams based on photographic meteors with mass, $M \geqslant 10^{-1}$ gram.

5. Gravitational and Body Shielding Factors

The gravitational and shielding effects of the Earth influence the actual flux that will be encountered by the HST. Thus, the sporadic flux model must be multiplied by a defocussing factor G to correct for the Earth's gravitational enhancement. The factor G is determined by

$$G = 0.43\ R/(R + H) + 0.57$$

where R is the radius of the Earth and H is the telescope's altitude above the surface of the Earth.

The gravitational effect of Earth on the flux of meteoroid streams is assumed to be negligible due to their high velocities.

The number of impacts as seen by a spacecraft shielded by the Earth is a function of its orientation with respect to the Earth. Assuming that the HST is randomly orientated, the actual number of impingements is the product of the unshielded, defocussed flux and the shielding factor S given by [1]:

$$S = 0.5\ (1 + \cos\theta) \quad ,$$

where $\sin\theta = R/(R + H)$.

Since the HST is not a convex object, i.e., not every surface element is exposed to 2π steradian, a shadowing effect will be present. As a result, some spacecraft components will have less exposure to the meteoroid environment than others. The degree of shadowing induced by the HST geometrical design can be determined from the Monte Carlo simulation results.

In order to simulate the telescope in its space environment, the HST geometrical model was positioned inside a sphere of radius 11 m and exposed to the simulated isotropic flux of sporadic meteoroids (Fig. A-4 in the Appendix). The effective surface area of the telescope was first estimated by running the Monte Carlo simulation and observing that 5487 trajectories intersected the model of the 28422 generated random chords in the sphere. This gives 293.5 m^2 as the estimate of the effective HST area with (286.6, 300.5) as a 95 percent confidence interval. Comparing this with the actual surface area of 316 m^2, it is concluded that the effect of shadowing is about 7 percent.

To simulate the meteoroid activity at the HST altitude of 590 km, the sporadic flux model was scaled by an Earth shielding factor of 0.70 and a gravitational defocussing factor of 0.96 to yield an expected flux of 5.46E-8 particles of mass 1E-6 grams or greater per second per square meter, or 1.61E-5 particles of mass 1E-6 grams or greater per second which strike the telescope. Thus, a meteor of mass in the range 1E-6 to 1 gram is expected to strike the HST every 17 hr, 14 min, 1.9 sec on the average.

To simulate a representative one-year profile of sporadic meteoroid impingements, the time in seconds between strikes is simulated as

$$t_i = -(1/1.61E\text{-}5)\ \ln U_i \quad ,$$

where

$$\sum_{i=1}^{k} t_i \leqslant 31536000 \quad \text{and} \quad \sum_{i=1}^{k+1} t_i > 31536000 \text{ sec.}$$

To simulate the time between strikes of a particular meteor stream, an average activity ratio F is computed for two consecutive days by linear interpolation of the models shown in Figure 12, and then the frequency is computed as

$$f = A\ 10^{-14.41}\ (1/m_c^{1.22})\ F\ (20/v)^4 \quad ,$$

where A is the effective area of the HST and v is the stream speed obtained from Table 2. The number 20 corresponds to the average sporadic meteoroid speed in the units, kilometers per second. Thus, the time between strikes for k hits in a 24 hr period is simulated as

$$t_i = -(\ln U_i)/f$$

with the constraint that

$$\sum_{i=1}^{k} t_i \leqslant 86400 \quad \text{and} \quad \sum_{i=1}^{k+1} t_i > 86400 \quad .$$

This completes the one-day simulation for one stream. This process is carried out for each of the 18 streams for each day of the year to yield a representative sample of the contribution of meteoroid strikes due to streams.

To obtain the angular momentum transfer to the vehicle by the i'th impinging sporadic meteoroid, one first simulates its speed v (km/s) from the probability speed distribution (Fig. 10) and its mass in grams as

$$m_i = \frac{m_c}{(1 - U_i\ (1 - m_c^{1.22}))^{1/1.22}} \quad ,$$

where m_c = 1E-6. This yields the magnitude of the meteor momentum as $m_i v_i$, which is then multiplied by the direction cosines of the i'th meteor trajectory to give the momentum vector.

Meteor stream velocities are obtained from Table 2 and stream masses generated as

$$m_i = \frac{m_c}{[1 - U_i (1 - m_c)]}$$

The angle of incidence that the meteor makes with the struck component surface will be an important consideration when computing the momentum transfer. Here the average incident component is modeled by observing that this will be

$$\int_0^{\pi/2} \cos\theta \, (d/d\theta \, \sin^2\theta) \, d\theta = 2/3 \quad ,$$

where $\sin^2\theta$ is the cumulative distribution function for the elevation angle and the integral gives the expected value of the momentum vector's perpendicular component to the impinged surface. This factor is of course slightly incorrect because of the shadowing effect, but is well justified in view of the simplification and saving in computer run time.

Thus, the normal component of the linear momentum vector of the incident meteoroid is taken to be $p = 2/3$ mv, where the average perpendicular component of the incident particle relative to the surface and the direction cosines of the meteoroid trajectory are included.

It should be noted that this approximation covers the horizontal component of the incoming momentum but neglects the horizontal component of the momentum of the ejecta, since no experimental data on this component is available.

D. Impact and Momentum Transfer

A model developed by Denardo and Nysmith [3] was used for the description of the momentum transferred to the HST by impacting meteoroids. Their model was based on experimental results in which aluminum spheres at speeds to 8 km/s impacted normally into an "infinitely thick" aluminum target. The model suggested by the data is given by:

$$(MV)_T = k \, (mv) \, d^{1/6} \, v^{1/3} \quad ,$$

where $(MV)_T$ is the momentum (ft lb/s) transferred to the target and mv is the momentum of the incident particle. The other factors which appear in the equation are:

d = projectile diameter, inches

v = speed of the projectile at impact, ft/s.

The factor k, which is referred to in Reference 3 as a constant in the correlation equation, necessarily has the units $(inch)^{-1/6}$ $(ft/s)^{-1/3}$. From the data presented in Table 1 of Reference 3, it was determined that k = 0.078. Application of this model in the meteoroid simulation required converting km/s into ft/s, grams into pounds; and, assuming a spherical shape and constant meteoroid density of 0.5 gr/cm^3, the simulated meteoroid diameter was converted from cm into inches. Having made these conversions, the momentum was computed and converted to N·m·s for use in the main program.

The momentum transfer equation predicts that with increasing velocity, the momentum ratio MV/mv grows beyond the value of two (starting at 32 km/s), which is the limiting value of classical impact theory. This is caused by the fact that target material is ejected from the impact crater at significant velocity.

In the present application, the momentum transfer indicated by this equation is taken as an approximate guideline, because the equation is correct only for the particular pellet/target material combination, and because of the extensive extrapolation involved when used at the meteoroid velocities.

Thus, for each impacting meteoroid, the angular momentum transfer vector is computed as

$$\underline{L} = \underline{r} \times 2/3\ k\ (m\ \underline{v})\ d^{1/6}\ |\underline{v}|^{1/3} \quad ,$$

where $\underline{r}$ is a vector whose components are the coordinates of the point of impact relative to a coordinate frame at the HST center of mass. The simulation was then run to yield a typical one-year profile of angular momentum transfers. Figure 13 depicts a year of simulated sporadic meteoroid strikes on the HST. The line segments emanating from the telescope represent the last part of the trajectories of the meteoroids up to and including impact. The length of these segments are proportional to the magnitude of their corresponding angular momentum vector. Note that many of the impacts which resulted in larger angular momentum transfers correspond to longer moment arms as one would expect.

The following is a breakdown of the sporadic meteoroid hits according to struck components:

Aft Shroud	164
Light Shield	127
Aperture Door	30
+X Solar Panel	91
-X Solar Panel	102
+X Solar Array Boom	1
-X Solar Array Boom	2
+Y High Gain Antenna (HGA) Boom	2
-Y HGA Boom	1
+Y HGA Hinge	0
-Y HGA Hinge	0
+Y HGA Dish	5
-Y HGA Dish	4
+Y HGA Feedhorn	0
-Y HGA Feedhorn	0
Secondary Mirror Baffle	0
Central Baffle	0
OTA Inner Wall	6
Primary Mirror	0
Total Number of Impacts	535

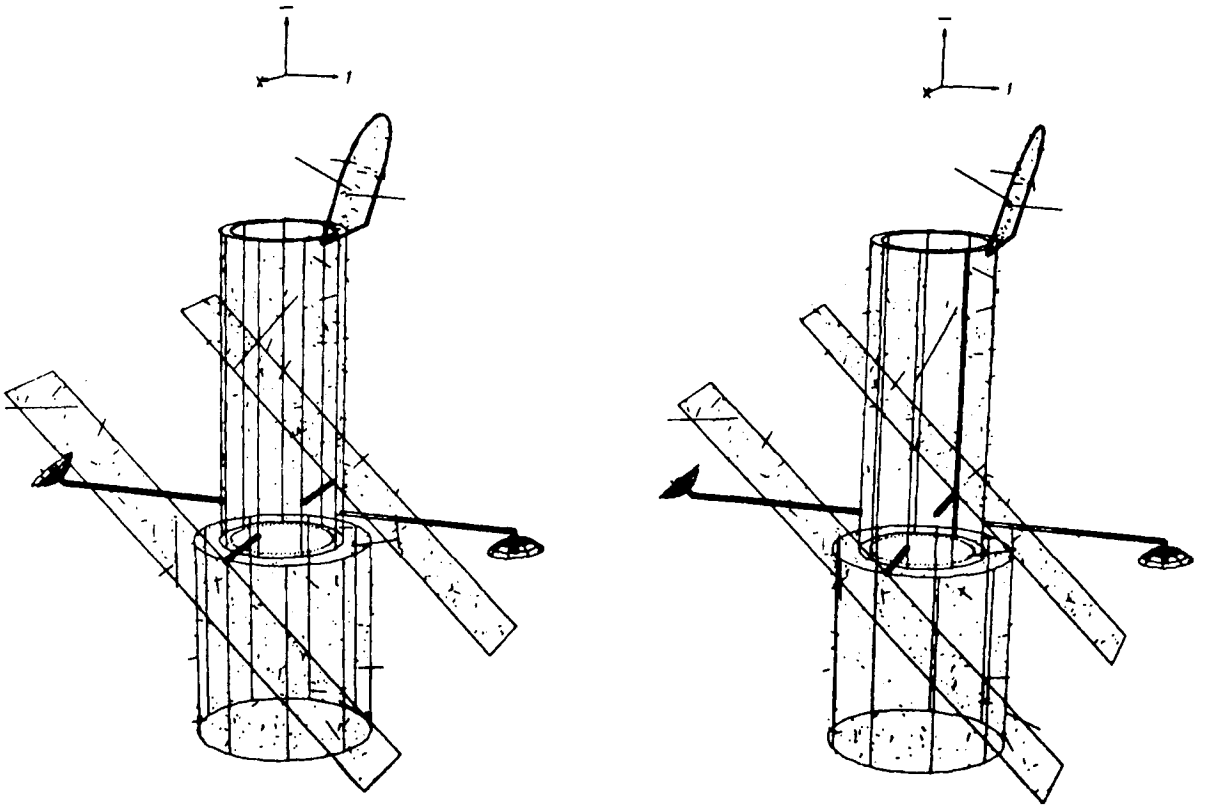

Figure 13. One year of simulated sporadic meteoroid strikes on the HST.

Figure 14 gives the components and magnitude of the angular momentum transfer vectors caused by the impacting sporadic meteoroids shown in Figure 13. Because the telescope is relatively insensitive to disturbances about the line-of-sight, the components L_x and L_y of the angular momentum transfer vector $\underline{L}$ and the magnitude of $(L_x^2 + L_y^2)^{1/2}$ are of primary concern. Figure 15 shows the magnitude of these two components for the one-year simulation of sporadic meteoroids. The horizontal line at 0.001 Nms is the threshold at which angular momentum transfers could cause a loss-of-lock. Note that there are 43 of the 535 (8 percent) sporadic meteoroid collisions exceeding the threshold.

Figure 16 depicts the angular momentum components L_x, L_y, L_z and the magnitude $|\underline{L}|$ caused by the 18 meteoroid streams. Figure 17 shows the corresponding magnitude of the x and y components which gives 13 of the 75 simulated stream meteoroid impingements which could cause a loss-of-lock.

E. Simulation Results

In the previous section, a simulation of meteoroid impingements was conducted which yielded a typical one-year profile of angular momentum transfers to the Hubble Space Telescope. Based on the sensitivity of the telescope to angular momentum transfers, about 8 percent of these meteoroid impacts can cause a loss-of-lock.

Since one-year simulated angular momentum transfer profiles will vary from computer run to run, it is of interest to approximate the probability distribution for these transfers, conditional on having a meteoroid impact. This can be achieved by simulating thousands of meteoroid impacts and then constructing the frequency histograms associated with the variables of interest.

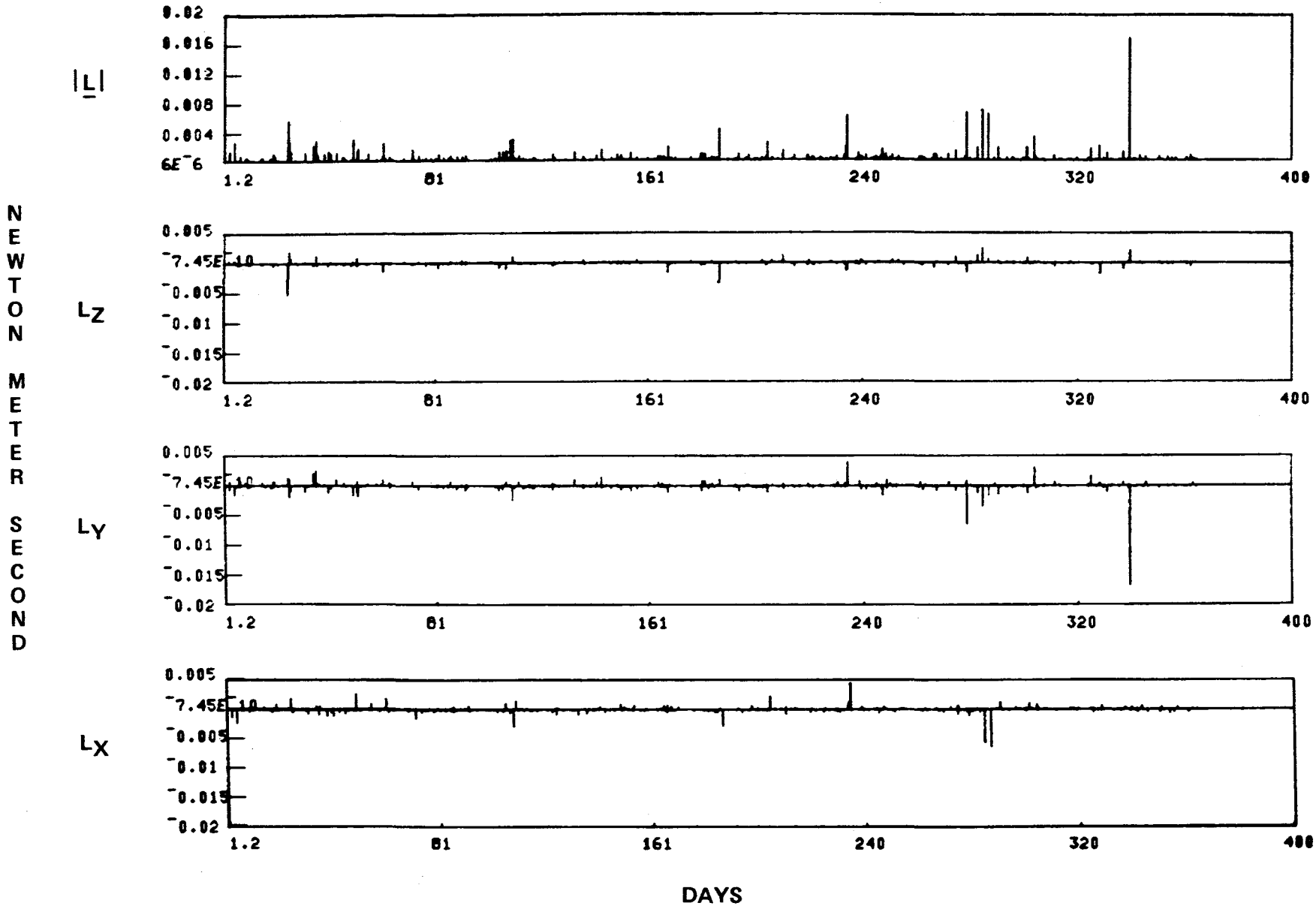

Figure 14. Angular momentum transfer vectors $\underline{L}$ for the sporadic meteoroids impacts in Figure 13.

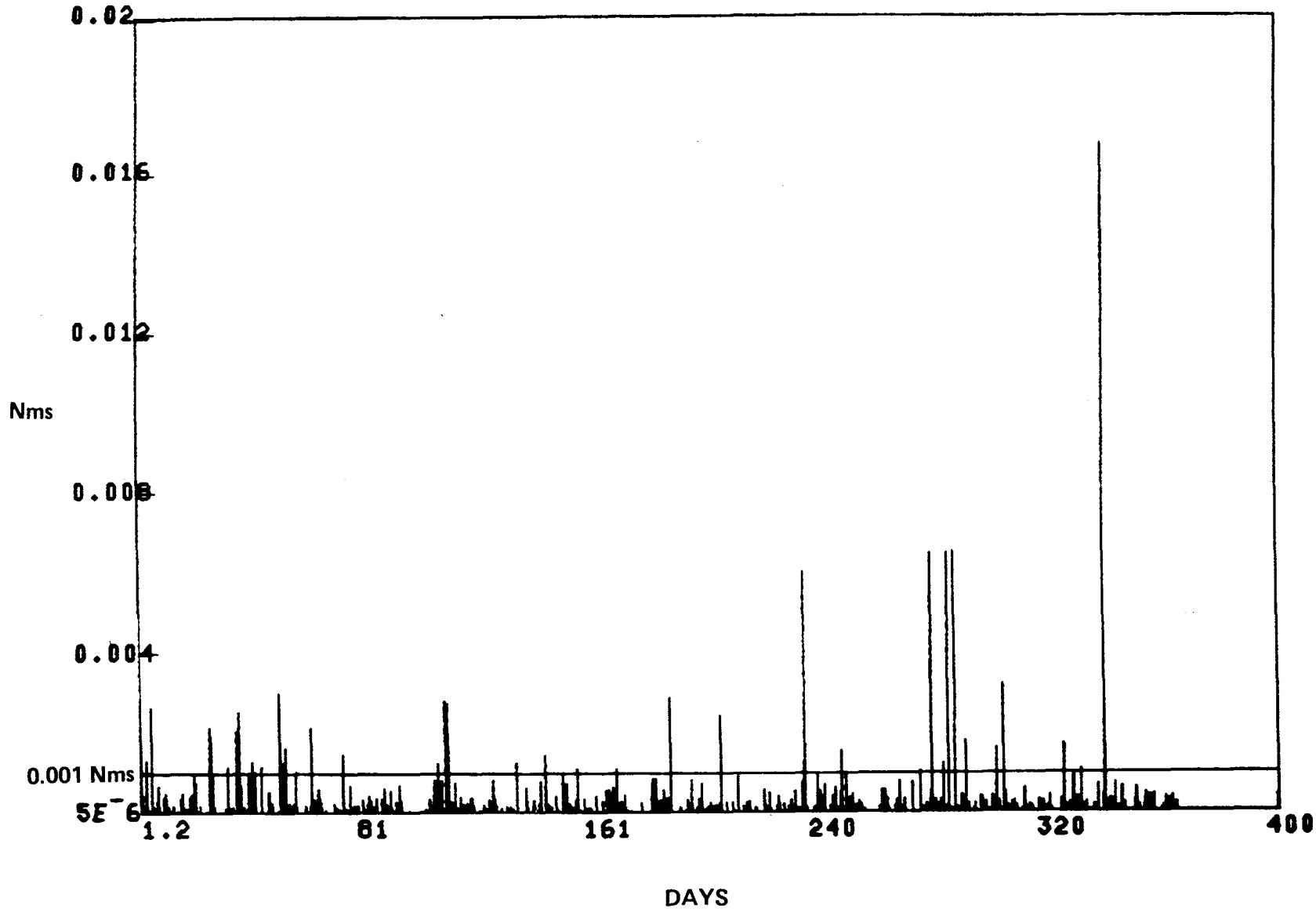

Figure 15. Magnitude of the x and y components $(L_x^2 + L_y^2)^{1/2}$ of the angular momentum transfers caused by sporadic meteoroid impacts.

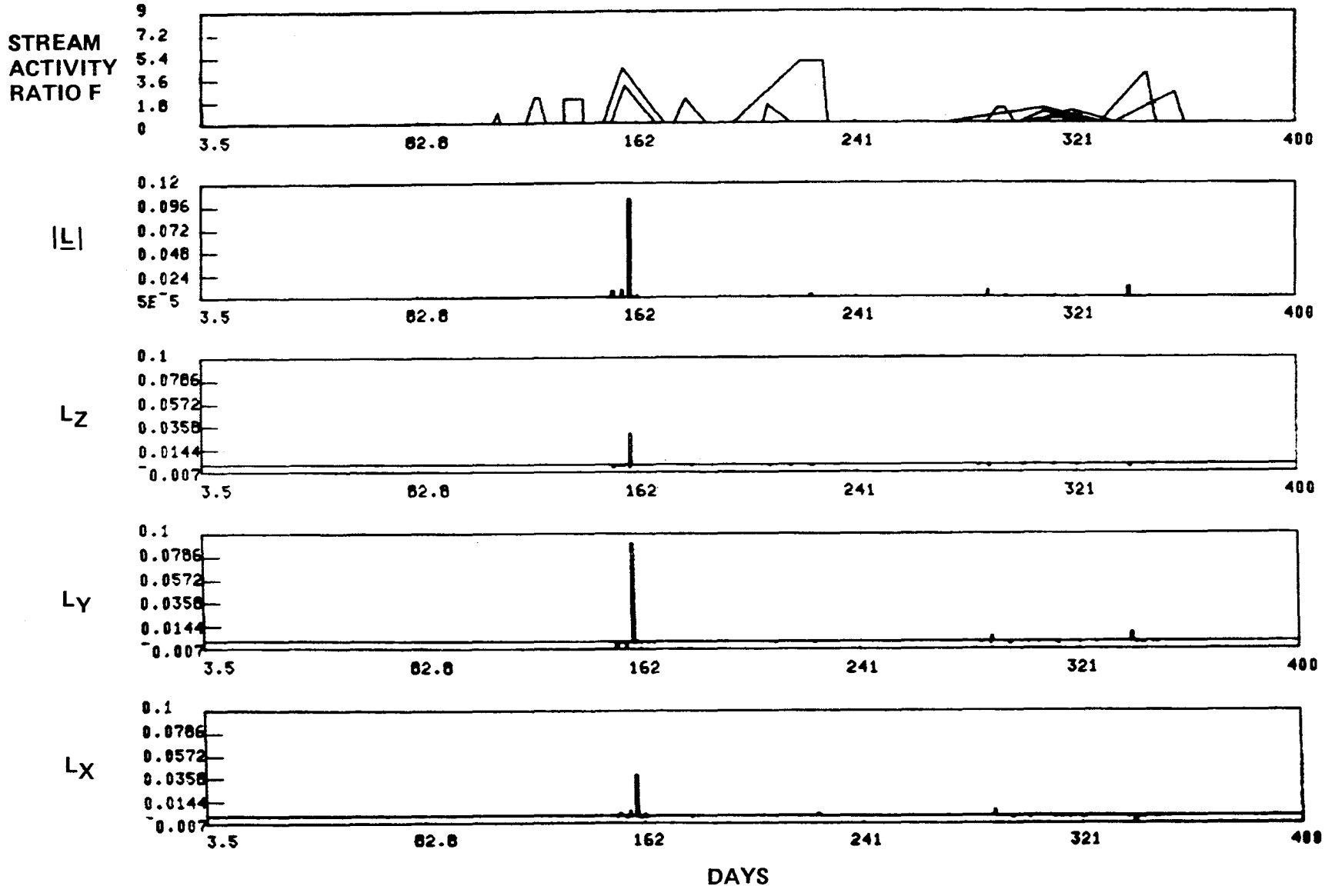

Figure 16. Angular momentum transfer vectors $\underline{L}$ (NMS) for stream meteoroid impacts.

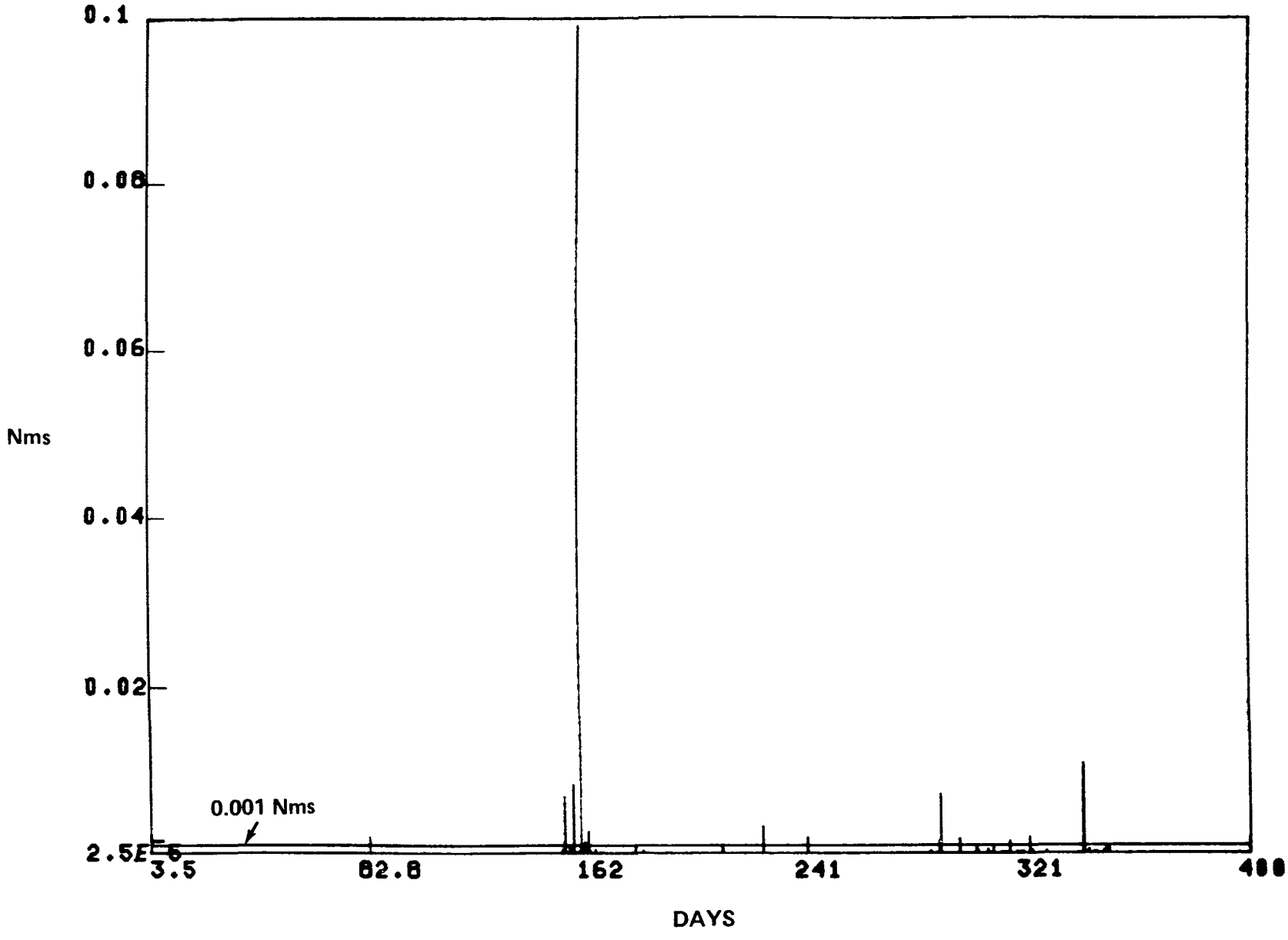

Figure 17. Magnitude of the x and y components $(L_x^2 + L_y^2)^{1/2}$ of the angular momentum transfers caused by stream meteoroid impacts.

Since a daily simulation is no longer required, the average cumulative meteoroid flux-mass model is used which combines the sporadic meteoroid flux with the stream meteoroid fluxes and is given by [1]:

$$\log_{10} N_t = -14.37 - 1.213 \log_{10} m, \quad 1E\text{-}6 \leqslant m \leqslant 1 \text{ gram},$$

where

N_t = number of particles of mass m or greater per square meter per second

m = particle mass in grams.

Also, since time is not a variable in the present approach, the gravitational defocussing factor and the Earth shielding factor are not included.

From the first computer run, 2806 impingements were obtained for the allocated run time with the following breakdown of impacts:

Aft Shroud	850
Light Shield	678
Aperture Door	146
+X Solar Panel	507
-X Solar Panel	510
+X Solar Array Boom	1
-X Solar Array Boom	5
+Y HGA Boom	9
-Y HGA Boom	7
+Y HGA Hinge	0
-Y HGA Hinge	0
+Y HGA Dish	35
-Y HGA Dish	22
+Y HGA Feedhorn	0
-Y HGA Feedhorn	0
Secondary Mirror Baffle	0
Central Baffle	0
OTA Inner Wall	35
Primary Mirror	1
Total Number of Impacts	2806

A breakdown of the impact coordinates according to struck component might be useful in the design of spacecraft when shadowing is of concern from the outset. This could feasibly be of interest when the accumulation of impingements has an eroding effect, such as on a telescope mirror, or when a particular module is very sensitive to particle impingements.

The impact coordinates of these meteoroids on the HST are depicted in the top-most stereo pair in Figure 18. Here one sees the outline of the telescope begin to take shape which is more obvious in

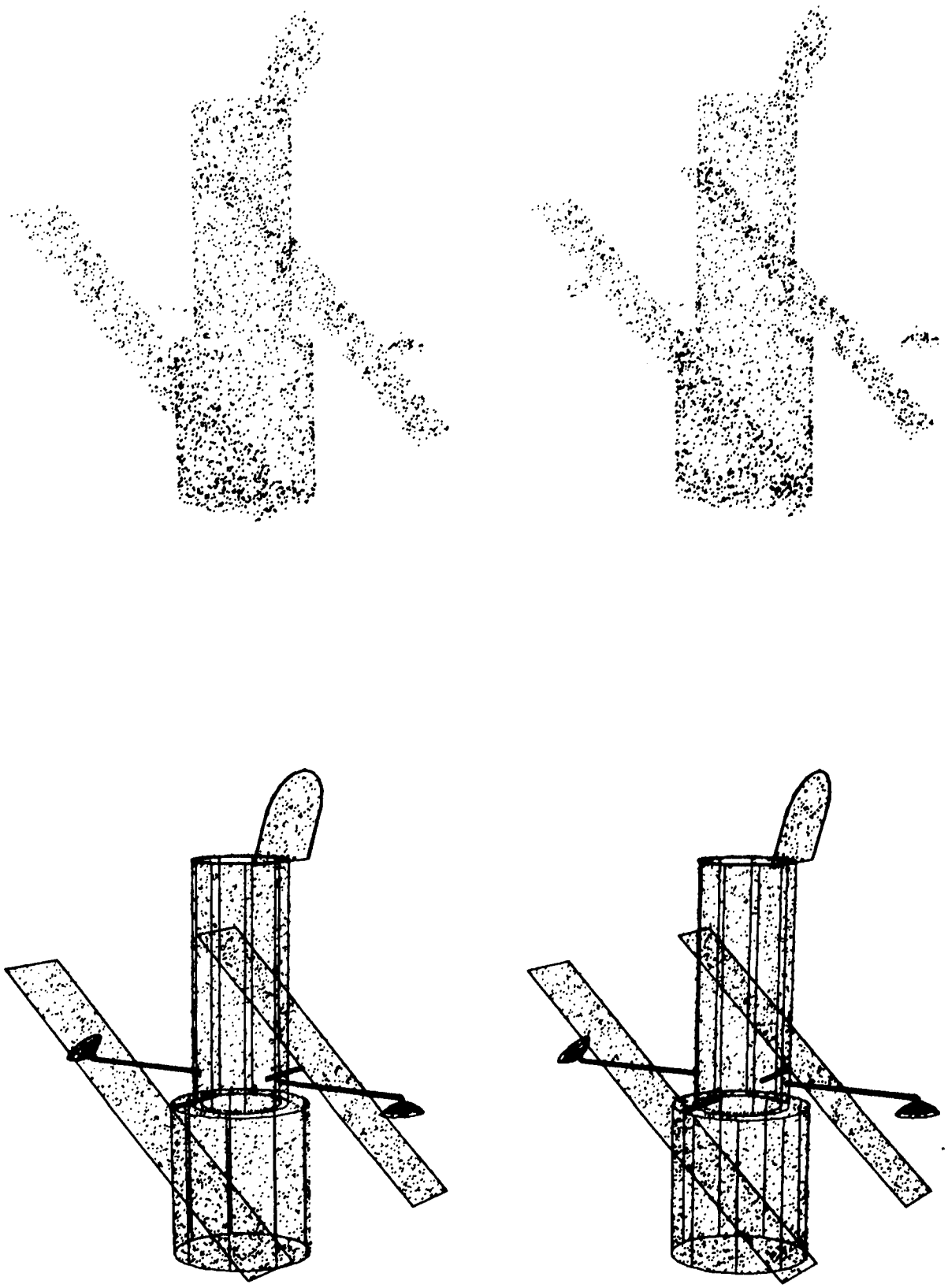

Figure 18. Meteoroid impact coordinates (top stereo pair) and with telescope included (bottom).

the bottom stereo pair where the outline of the telescope has been included. A fairly uniform distribution of impacts over the surface of the telescope (and no false impacts) combined with a reasonable breakdown of impacts by struck component gives a certain degree of confidence in the programmed model.

A plot of the x and y components of the associated angular momentum transfer vectors is given in Figure 19(a) from which a two-dimensional histogram may be constructed. Running the program again and obtaining enough simulation data to get a fairly smooth surface, the bivariate histogram is constructed in Figure 19(b). In this figure, the limits

$$-0.004 \leqslant L_x \quad , \quad L_y \leqslant 0.004 \text{ NMS}$$

have been used so that more detail in the bivariate density function can be seen. This histogram approximates the bivariate probability distribution for the x and y components of angular momentum transfers, given the event of a meteoroid impingement.

Since telescope pointing disturbances can result when the magnitude of the x and y components exceeds 0.001 Nms, the probability density function for $(L_x^2 + L_y^2)^{1/2}$ is approximated in Figure 20, where transfers greater than 0.004 Nms have been omitted from the graph for display purposes.

This is the simulated probability density function for the magnitude of the x and y components of the angular momentum transferred to the Hubble Space Telescope from impinging meteoroids in the mass range 1E-6 to 1 gram.

This distribution can be combined with the distribution of the time between hits or the distribution for the number of hits per time interval T to give the expected number of disturbances and other statistical results of interest.

Using the cumulative distribution function of the simulation data, it is found that 5 percent of the impingements can cause a pointing disturbance. This is somewhat lower than the 8 percent observed in the one-year simulation and it is concluded that the one-year profile represents a more turbulent year than normal.

IV. CONCLUSION

A general methodology is developed for performing a Monte Carlo simulation of particles impinging on an orbiting spacecraft.

Using generic shapes, a spacecraft geometrical model is constructed with the level of detail being dependent upon the simulation objective. This geometrical model is then suspended inside a region of space, e.g., a sphere, and the particle flux simulated within the region. Points of impact on the geometrical model are determined and the resulting physical events of interest are modeled, based on the characteristics of the impinging particles and the spacecraft material. Simulation data is maintained throughout the computer run from which statistical inferences about the variables under investigation can be made.

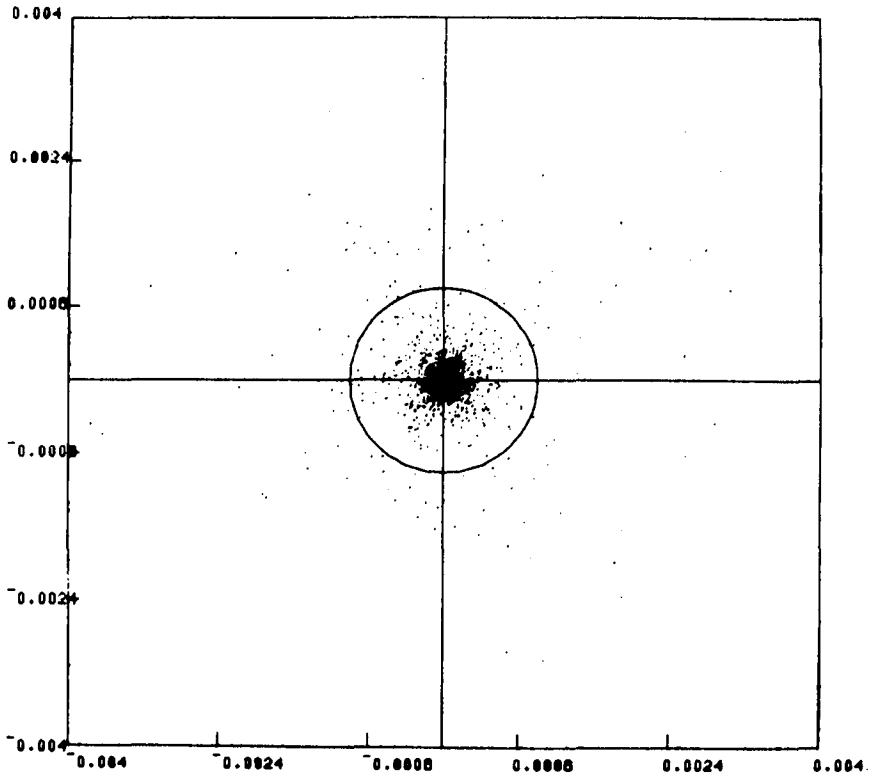

Figure 19(a). Plot of the x and y components of the angular momentum transfer vectors.

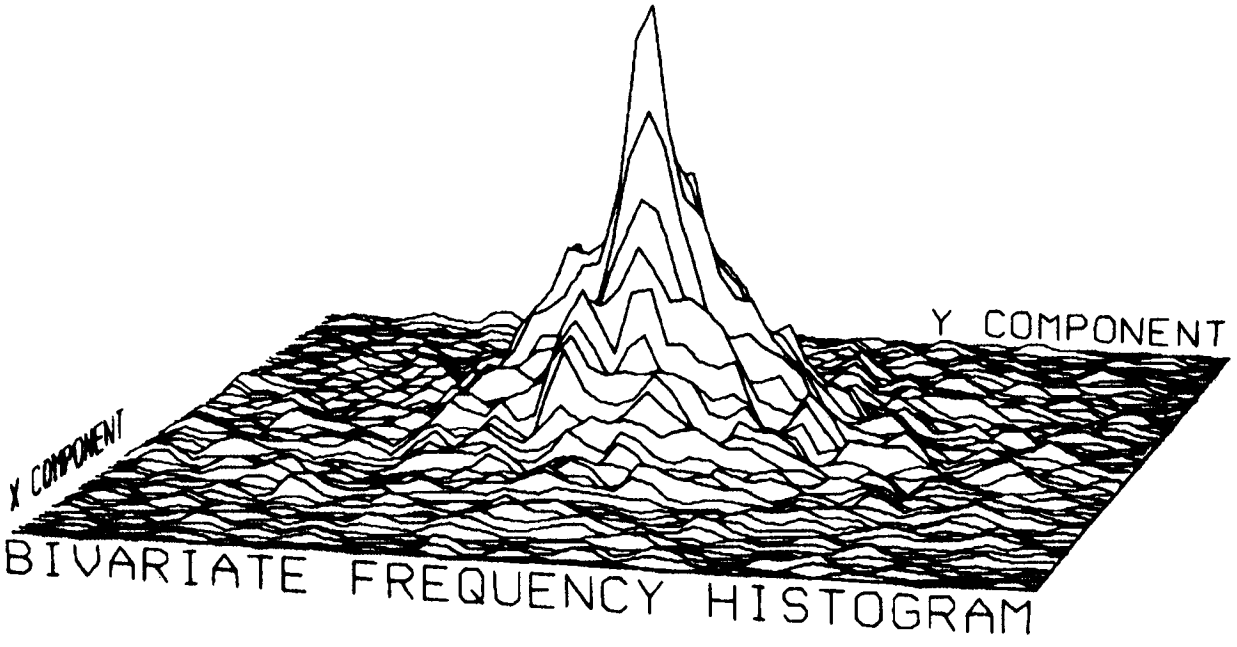

Figure 19(b). Bivariate frequency histograms of the x and y components of the angular momentum transfer vectors.

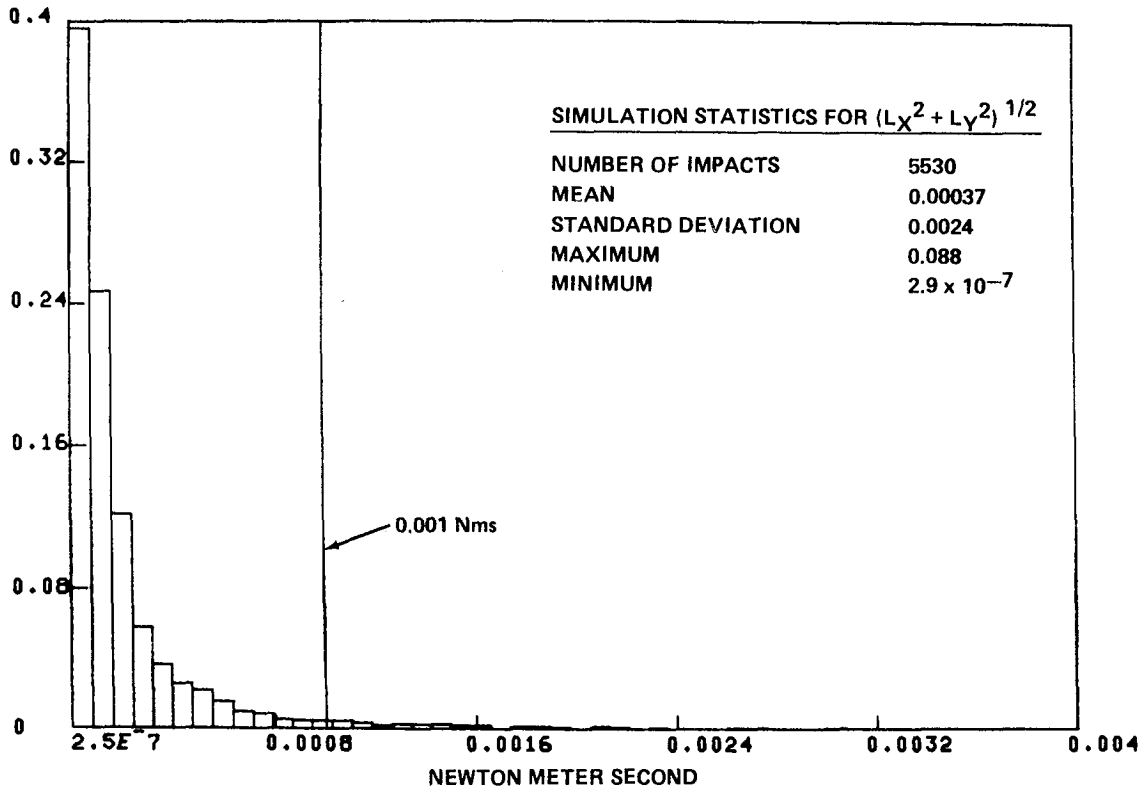

Figure 20. Probability density function for the magnitude $(L_x^2 + L_y^2)^{1/2}$ of the angular momentum transfer vector.

A study of the Hubble Space Telescope in the micrometeoroid environment of its planned Earth-orbit and the threat of impingement induced pointing disturbances is presented to illustrate this methodology.

APPENDIX A

STEREO VISUALIZATION WITHOUT OPTICAL AIDS[3]

(Cross-Eyed Stereo)

On many occasions in engineering and physical analysis, it would be useful to be able to sketch in three dimensions. To fulfill this wish in many cases, a convenient technique which requires no optical devices other than one's eyes may be used. All that is required is a stereoscopic pair of images. One additional capability is necessary. The observer must be able to cause the lines of sight of his eyes to converge; i.e., one must cross one's eyes. The stereo projections are formed as shown in Figure A-1. The images are reversed and viewed as in Figure A-2. With a little practice, one can easily learn to reconstruct mentally, the 3-dimensional scene from the reversed stereo pairs. In this report there are two stereo pictures. The interested reader should try several viewing distances. (The farther away the page the less crossing of the eyes is required and the easier it becomes to focus the images.) Squinting may also help as it increases one's depth of focus. When one first looks at a stereo pair, one focuses on the page and sees two similar but separate images. As one begins to cross his eyes, the two images become four. Continue crossing the eyes until the interior pair of images come together. Since the line connecting corresponding points on the images must be at the same angle about the line of sight as the line connecting the eyes, it may be necessary to rotate the page or rock the head until these two images become superimposed and seem to merge into a stereo image. This technique does require some practice but once mastered it can be very useful for easy visualization in 3 dimensions.

If a computer with plot capability is available, we can construct the necessary stereo projections from a set of points and lines that represent the object of interest. We have referred to such a representation as a wire frame model because of the appearance of the image. Let P be a representative point of the model. Each point P is projected into the picture plane S as shown in Figure A-3. The point P is projected to the eyepoint E and the line PE intersects the picture plane S at P′. P′ is the projection of P onto S. The set of all points P′ projected from object points P together with the connecting lines form the desired projection. We set up a reference frame in the plane S. To do this, we must specify which way is up (so to speak). Let $\underline{u}_u$ be a unit vector in this direction and $\underline{u}_r = \underline{u}_u \times \underline{\ell}$ is a unit vector in S pointing to the right. We place the origin of the S coordinate reference at O. Observe that $\underline{r}_O = \underline{r}_E + d\,\underline{\ell}$; where $\underline{r}_O$ and $\underline{r}_E$ are position vectors of O and E, respectively. From the geometry shown in Figure A-3, we can see that

$$\underline{r}_{P'} = \underline{r}_E + (\underline{r}_P - \underline{r}_E)\, d/\underline{\ell} \cdot (\underline{r}_P - \underline{r}_E) \quad .$$

From this we can compute

$$x_{P'} = (\underline{r}_{P'} - \underline{r}_O) \cdot \underline{u}_r$$

$$y_{P'} = (\underline{r}_{P'} - \underline{r}_O) \cdot \underline{u}_u \quad .$$

Since $\underline{\ell} \cdot \underline{u}_u = \underline{\ell} \cdot \underline{u}_r = 0$,

3. Extracted from NASA TM-78252, Torque Equilibrium Attitude Control For Skylab Reentry, Nov. 1976, by John R. Glaese and Hans F. Kennel.

$$x_{P'} = (\underline{r}_{P'} - \underline{r}_E) \cdot \underline{u}_r$$

$$y_{P'} = (\underline{r}_{P'} - \underline{r}_E) \cdot \underline{u}_u \quad .$$

The set of points $(x_{P'}, y_{P'})$ plotted conventionally forms the desired projection. Size can be altered by scale adjustments. These projections are then placed as desired. Also, the values used for d and eye separation s are arbitrary and can be adjusted for convenience or eye comfort. In real life s ≅ 65 mm and d ≅ 250 mm for comfortable reading; however, it may be more comfortable for d to be larger. Some initial experimentation with this technique should establish desirable settings.

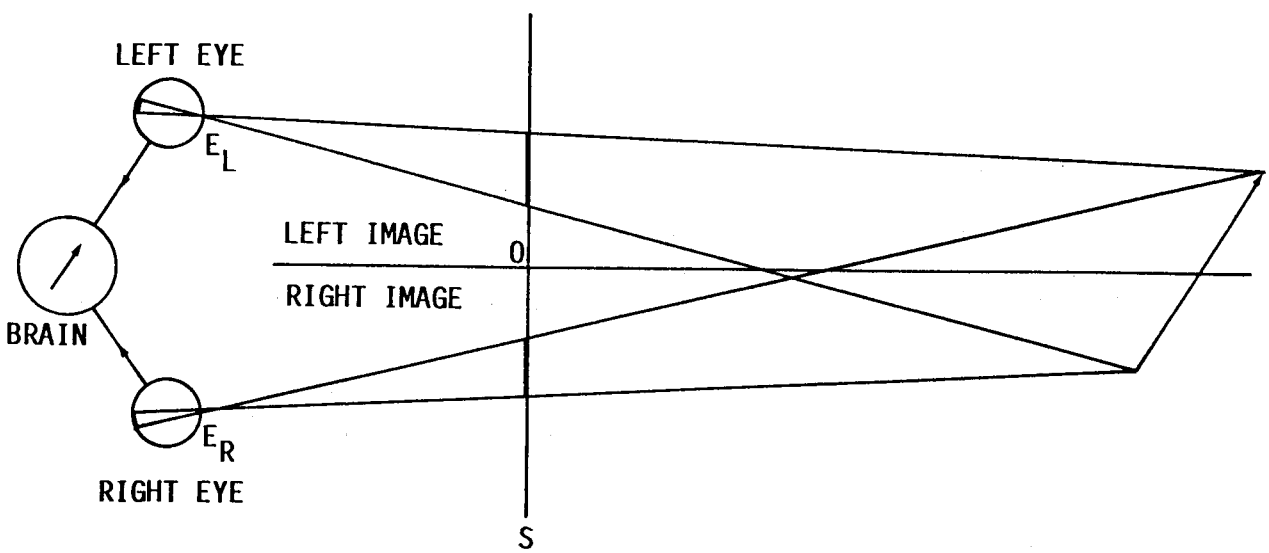

Figure A-1. Stereo projection.

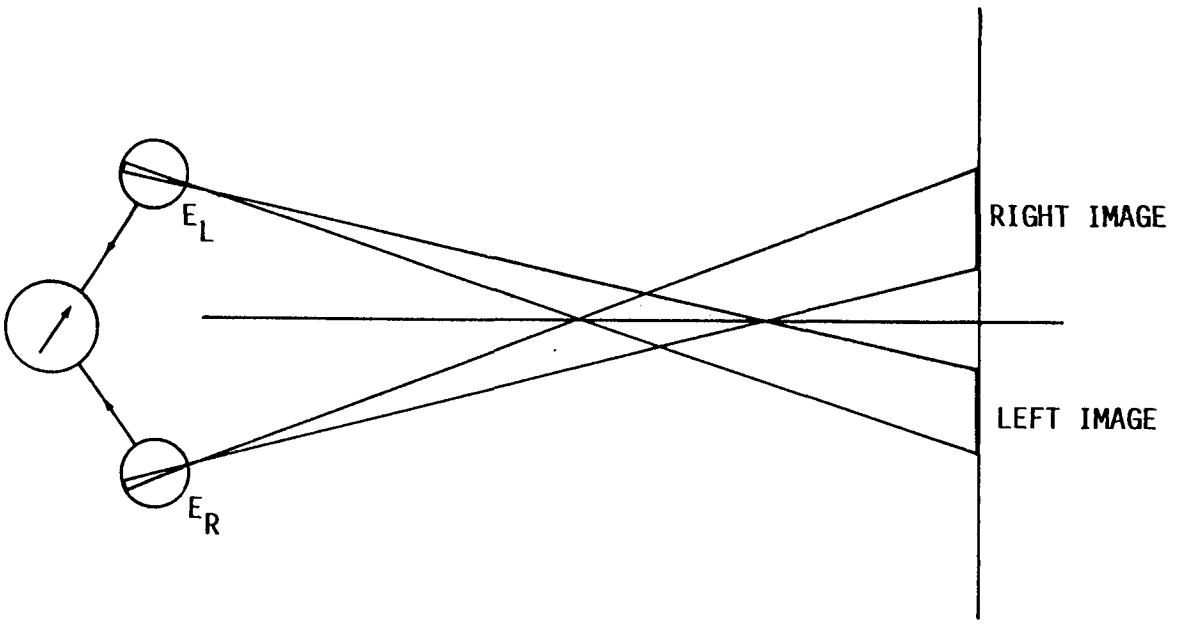

Figure A-2. Stereo reconstruction by cross-eyed viewing.

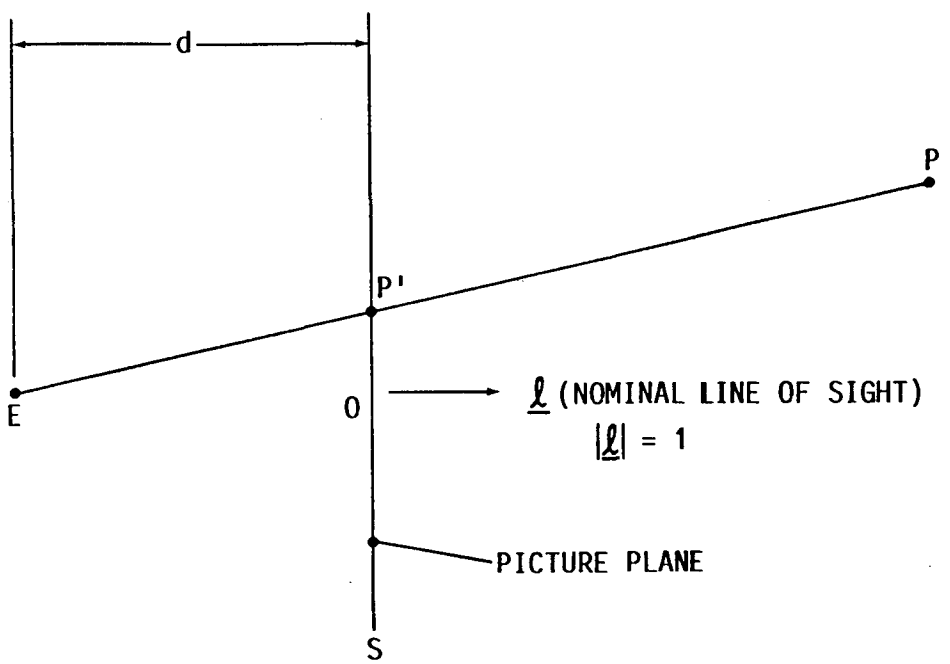

Figure A-3. Projection geometry.

Hint to Stereoscopic Viewing

Hold the stereoscopic pair at arms length and then focus on a point about half way in-between. As an aid, try looking at your fingertip placed in the line of sight such that when your left eye is closed, your right eye sees your fingertip at the center of the left hand figure. Now, with your right eye closed, check that your left eye sees your fingertip at the center of the right hand figure. This will locate the focal point for cross-eyed stereo viewing. Now, with both eyes open, look at this point in space. At first, you will find it helpful to just stare at your fingertip. Then, in the background, you will notice three images. Try to shift your concentration from your fingertip to the middle image, which will begin to look sharp and clear (and three-dimensional). Once you have locked in on the object, remove your fingertip. With a little practice, one can easily master this technique. Figure A-4, which represents the telescope inside a sphere with some particle trajectories, is a good stereoscopic pair to get started on because it is very three-dimensional.

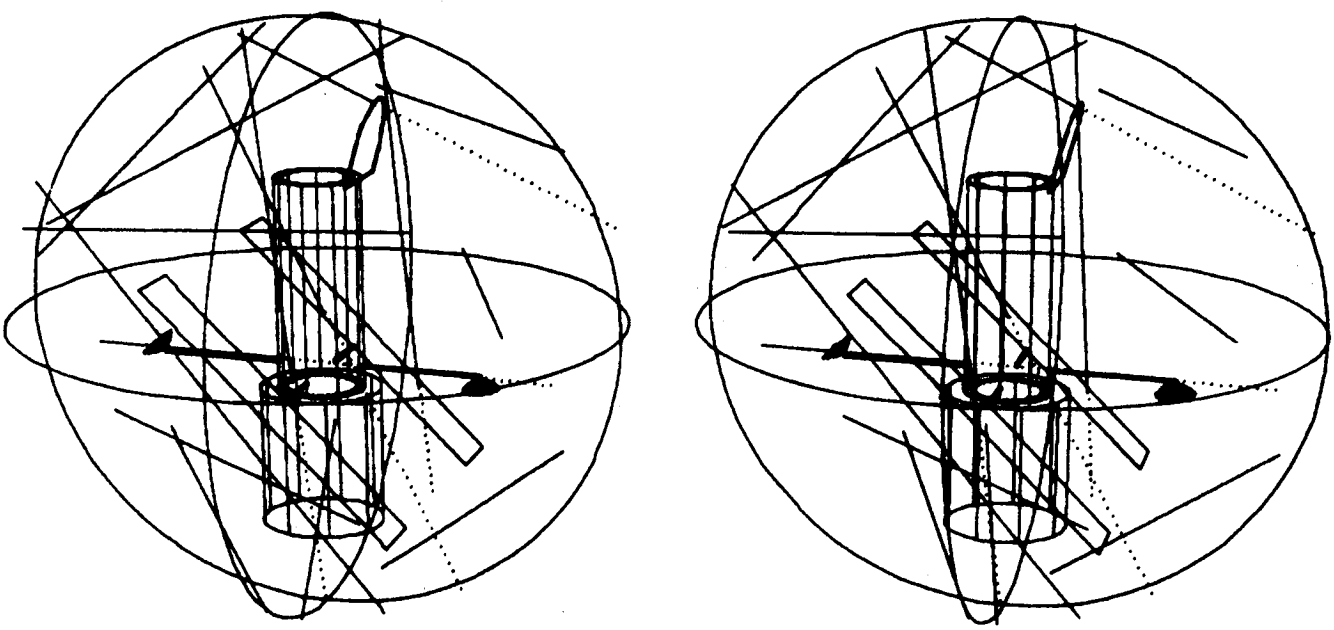

Figure A-4. Simulation of the meteoroid environment inside a sphere containing the Hubble Space Telescope.

REFERENCES

1. Cour-Palais, B. G.: Meteoroid Environment Model – 1969 (Near Earth to Lunar Surface). NASA SP-8013, March 1969.

2. Howell, L. W., and Kennel, H. F.: A Stochastic Model for Photon Noise Induced by Charged Particles in Multiplier Phototubes of the Space Telescope Fine Guidance Sensors. NASA TP-2337, June 1984.

3. Denardo, B. P., and Nysmith, R.: Momentum Transfer and Cratering Phenomena Associated with the Impact of Aluminum Spheres Into Thick Aluminum Targets at Velocities to 24,000 Feet Per Second. AGARDograph 87, Vol. 1, pp. 389-402, The Fluid Dynamic Aspects of Space Flight. Gordon and Breach Science Publishers, New York, 1964.

1. REPORT NO.	2. GOVERNMENT ACCESSION NO.	3. RECIPIENT'S CATALOG NO.
NASA TP-2550		

4. TITLE AND SUBTITLE	5. REPORT DATE
A Stochastic Model for Particle Impingements on Orbiting Spacecraft	January 1986
	6. PERFORMING ORGANIZATION CODE
7. AUTHOR(S)	8. PERFORMING ORGANIZATION REPORT #
Leonard W. Howell, Jr.	
9. PERFORMING ORGANIZATION NAME AND ADDRESS	10. WORK UNIT NO.
George C. Marshall Space Flight Center Marshall Space Flight Center, Alabama 35812	M-507
	11. CONTRACT OR GRANT NO.
	13. TYPE OF REPORT & PERIOD COVERED
12. SPONSORING AGENCY NAME AND ADDRESS	Technical Paper
National Aeronautics and Space Administration Washington, D.C. 20546	14. SPONSORING AGENCY CODE

15. SUPPLEMENTARY NOTES

Prepared by Systems Dynamics Laboratory, Science and Engineering Directorate.

16. ABSTRACT

A general methodology for simulating particle impingements on orbiting spacecraft is developed. Major steps in the modeling process are presented as (1) modeling objective, (2) construction of the spacecraft geometrical model, (3) simulation of the particles in the space environment, (4) particle impact and subsequent events of interest, and (5) results of the simulation.

A simulation of the expected meteoroid impingements on the Hubble Space Telescope and the resulting angular momentum transfers which can cause telescope pointing disturbances is given to illustrate these methods.

17. KEY WORDS	18. DISTRIBUTION STATEMENT
Angular Momentum Transfer Cosmic Rays Hubble Space Telescope Meteoroids Monte Carlo Simulation Photon Noise Space Environment	Unclassified - Unlimited Subject Category 65

19. SECURITY CLASSIF. (of this report)	20. SECURITY CLASSIF. (of this page)	21. NO. OF PAGES	22. PRICE
Unclassified	Unclassified	42	A03

For sale by National Technical Information Service, Springfield, Virginia 22161

NASA-Langley, 1986

National Aeronautics and
Space Administration
Code NIT-4

Washington, D.C.
20546-0001